Toward NLFEA-based fragility curves for unreinforced masonry buildings exposed to subsidence

Prosperi, Alfonso; Korswagen, Paul A.; Longo, Michele; Korff, Mandy; Rots, Jan G.

DOI
10.1016/j.jobe.2025.113676

Publication date
2025

Document Version
Final published version

Published in
Journal of Building Engineering

Journal of Building Engineering 112 (2025) 113676

Contents lists available at ScienceDirect

Journal of Building Engineering

journal homepage: www.elsevier.com/locate/jobe

Toward NLFEA-based fragility curves for unreinforced masonry buildings exposed to subsidence

Alfonso Prosperi [a,*], Paul A. Korswagen [a], Michele Longo [a], Mandy Korff [a,b], Jan G. Rots [a]

[a] Delft University of Technology, Faculty of Civil Engineering and Geosciences, Stevinweg 1, Delft/2600 GA, Delft, 2628 CN, the Netherlands
[b] Deltares, P.O BOX, 177, 2600 MH, Delft, the Netherlands

ARTICLE INFO

Keywords:
Finite elements
Fragility curves
Unreinforced masonry
Settlement
Subsidence
Damage
Cracks

ABSTRACT

Subsidence caused by natural or human-induced factors can occur unevenly, resulting in differential settlements. Existing unreinforced masonry (URM) buildings are susceptible to damage from differential settlements. However, the extent of the damage varies between structures, depending on factors such as the magnitude and pattern of the settlements, along with the features of the building and the properties of the underlying soil. Non-linear finite element analyses (NLFEA) are often used for studying the damage response, accounting for variability in soil and structural features. This study uses 6912 NLFEA, including 8 variations in façade geometry, 3 masonry materials, 2 soils, 2 shallow foundation systems, and 72 settlement patterns, to develop fragility curves for URM buildings undergoing subsidence. Old Dutch URM buildings with strip foundations are modelled using 2D plane-stress façade models, accounting for non-linear smeared shearing, cracking and crushing of masonry and 3D effects of transverse walls. Settlement troughs are applied at a non-linear soil-foundation interface, with angular distortion (β) progressively increasing to quantify settlement intensity and building deformation. As β increases, the NLFE models exhibit progressive cracking damage, with severity objectively assessed through the parameter Ψ considering crack width, length, and number. Then, the distortion β is used as the demand parameter to develop the fragility curves. The analysis shows that long façades are twice as likely to experience 5 mm cracks from settlement damage compared to short façades under an applied β of 2 ‰ (1/500). For this applied β, proposed as an acceptable limit for many structures in the Eurocode, half of the models exhibit cracks up to 5 mm wide. Therefore, while 1/500 may be considered safe for structural integrity, it can still lead to noticeable damage. Light damage occurs even at angular distortion values below 0.5 ‰ (1/2000), with 10 % of models showing cracks up to 1 mm wide.

1. Introduction

1.1. Underlying concepts

Land subsidence is the downward movement of the ground surface due to natural or human-induced drivers, classified as deep

* Corresponding author.
E-mail address: a.prosperi@tudelft.nl (A. Prosperi).

https://doi.org/10.1016/j.jobe.2025.113676
Received 2 April 2025; Received in revised form 1 July 2025; Accepted 2 August 2025
Available online 5 August 2025

(below 50 m) or shallow. Subsidence affects different areas worldwide, such as North America, China, Vietnam, and, in particular, the Netherlands. When subsidence occurs unevenly, it results in differential settlements, which can lead to damage to existing buildings. Unreinforced masonry (URM), having limited tensile strength, is especially vulnerable to differential settlements that induce cracks in walls, potentially affecting the aesthetics, functionality, and/or safety of buildings.

In the Netherlands, 80 % of the 10 million buildings are estimated to be built with URM [4], with around 50 % built before 1975 (Fig. 1). Structures built before WW2 often feature double wythe walls with timber diaphragms used for the floors and roof. After 1945, cavity walls and concrete floors have increasingly been adopted [5]. Before 1960, both the inner and outer leaves of the cavity walls were made mainly of single-wythe clay bricks, whereas afterwards, calcium-silicate bricks and blocks were used for the load-bearing inner leaf [5,6]. The veneer of cavity walls is typically non-loadbearing. A nationwide dataset (© 3DBAG by tudelft3d and 3DGI [7]) provides height data from various sources [8], which has been used in prior research to study the geometrical features of 53 million exterior walls [1,2]. As shown in Fig. 2, most walls fall within the height range typical of low-rise (one to three storeys) structures.

Approximately 70 % of Dutch buildings are expected to have shallow foundations, 5–6 % timber piles, and the remainder concrete piles [9]. Buildings on piles are less affected by subsidence, as they reach deeper, more stable soil layers, while buildings on shallow foundations are directly exposed to settlements. Strip foundations, the most common type of shallow foundation until 1925 and less frequently used until the 1970s [10], were typically made of URM. The wall width progressively increases (up to 1–1.5 m) with depth, reaching up to 2 m below the ground surface. More recent structures commonly use reinforced concrete (RC) foundations, with masonry walls resting on reinforced concrete slabs or thick strips.

The relationship between ground settlement and building damage has been extensively studied through in-situ observations, physical experiments, numerical simulations, or their combination [11]. Early research introduced settlement metrics such as differential settlement, angular distortion, rotation, deflection ratios, and horizontal strains, along with semi-empirical thresholds that are widely adopted in international guidelines [12–15]. More recent work has used experiments and numerical models to assess structural response and damage due to settlement, enabling controlled variation of factors such as building type, material properties, and settlement patterns [16–31]. However, experimental testing is often limited by time and cost, while numerical modeling provides a more flexible and efficient alternative. Nonlinear finite element analyses (NLFEA) have been widely employed to simulate the complex interaction between soil, foundation, and structure, including the cracking behavior of quasi-brittle materials such as URM when subjected to differential settlements [10,17,22–25,29,32–35]. For a comprehensive review of the literature, the reader is referred to Refs. [11,36,37]. Advancements in computational performance now make it possible not only to assess the response of individual structures but also to conduct large numbers of simulations to characterize the probabilistic behavior of buildings, which is the primary focus of this study.

1.2. Research goal

In this research, NLFEA are used to simulate the response of URM buildings subjected to subsidence, aiming to characterize the probabilistic response of existing buildings via fragility curves. The NLFEA incorporate both structural and soil characteristics, enabling the characterization of cracking damage under increasing differential settlement [10,29,38,39].

The analysis targets URM buildings on strip foundations built before 1970. This study focuses on differential settlements resulting from subsidence caused by shallow drivers (within the first 50 m of the subsurface), such as groundwater fluctuations, peat oxidation, and groundwater absorption, whereas tunnelling, mining, and excavation, already extensively studied in prior research, are not the focus.

This paper begins with Section 2 (Methodology and NLFE models), outlining the approach adopted to derive the fragility curves based on the numerical analyses. Section 3 (Results) presents the results of the analyses, whereas Section 4 focuses on the NLFE-based

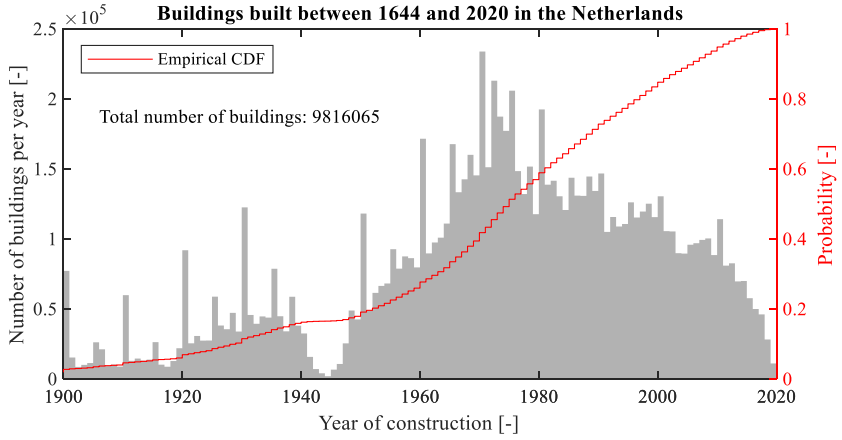

Fig. 1. Histogram of the year of construction for existing buildings in the Netherlands available in the BAG3D database [1,2]. The data refers to the existing buildings identified as "in use" ("*pand in gebruik*", in Dutch [3]). The data for buildings that have been demolished is not available.

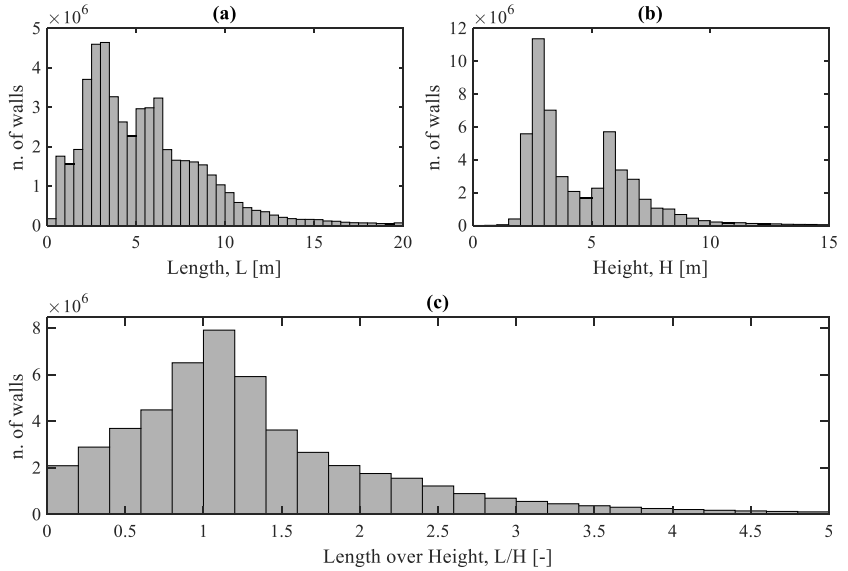

Fig. 2. Histograms of the walls' length (a) and height (b). (c) shows the length-over-height ratio.

fragility curves. Section 5 (Discussion) discusses the results and compares them with previous research. Finally, Section 6 (Conclusions) summarises the key findings.

2. Methodology and NLFE models

2.1. Analysis procedure

The analysis procedure comprises three steps (Fig. 3). In Step 1, 8 façade geometries (including variations in wall shape, dimensions, and openings), 3 masonry materials, 2 soils, and 2 shallow foundations are selected to represent Dutch residential low-rise buildings, specifically detached and semi-detached URM houses built before 1970.

The selected façades are used to build 2D plane-stress NLFE models with the software DIANA FEA 10.8 [40]. The modelling strategy, adopted in previous studies (e.g., Refs. [10,17,21,22,29,39]), employs a semi-coupled 2D structural model of the façade and foundation, incorporating the non-linear smeared shearing, cracking and crushing behaviour of masonry in a homogenized continuum. At the bottom of the foundation, a non-linear interface is used for the soil-structure interaction. The models include the effects of the transversal walls. 72 symmetric and asymmetric sagging and hogging greenfield settlement shapes are then imposed at the bottom of the model. The intensity of the settlement is characterized using angular distortion β, i.e., the slope of the line connecting two points

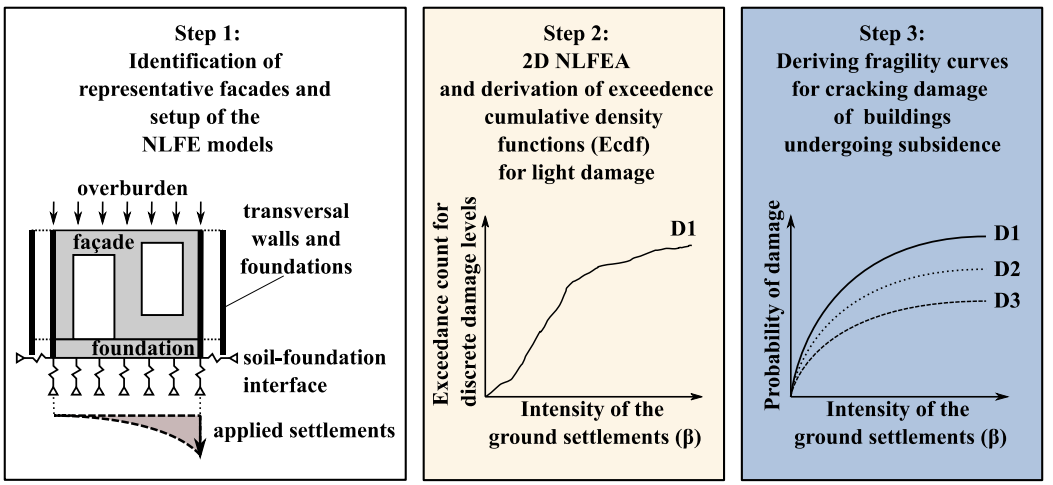

Fig. 3. The methodology adopted in this study.

relative to the tilt of the building [15]. The imposed β is progressively increased, and the structure's cracking response is tracked. While in prior research damage due to settlement is often assessed by considering the width of cracks [17,18,20,22,27,41], in this study the damage parameter Ψ [28,42] is used to quantify the damage, considering the number of cracks, their width and length. The NLFEA are further detailed in Section 2.2.

In Step 2, the results of the NLFEA are used to retrieve the exceedance cumulative density functions (ECDF), with β as the demand parameter for discrete Ψ values. As β increases, the ratio of models reaching specific Ψ determines the ECDF, revealing the probability of damage. The obtained ECDF are used to explore the influence of the selected building and soil features.

Finally, in Step 3, fragility curves are obtained. Fragility curves are cumulative distribution functions that relate damage severity to the hazard intensity [43,44]. One of the most widely used forms is represented by the two-parameter lognormal distribution function in equation (1), which guarantees no negative probabilities [36,45]:

$$F(SRI_i, \zeta_i) = \Phi\left[\frac{1}{\zeta_i}\ln\left(\frac{SRI_i}{\overline{SRI_i}}\right)\right] \quad (1)$$

Where SRI_i represents the "settlement-related intensity" of the *i-th* case, while $\overline{SRI_i}$ and ζ_i, respectively representing the median and the standard deviation (or dispersion) of the lognormal distribution. Finally, $\Phi[\cdot]$ is the standardized normal distribution function. The parameters while $\overline{SRI_i}$ and ζ_i are obtained by fitting the ECDF, which includes the results of all NLFEA simulations, ensuring the reproducibility and ease of use of the fragility curves.

2.2. Setup of the NLFEA

2.2.1. Selection of the façade geometries

Eight façades of old clay-baked masonry buildings are selected from previous studies ([46–48]) and shown in Fig. 4. Table 1 summarises the main geometrical features of the façades and their transversal walls. Six façades are double-wythe walls, whereas only two façades are single-wythe (Table 1). Masonry lintels are used for the openings in most cases (Fig. 4 ie., for the façades herein labelled as "FA", "FC", "FD", "FE", "FF"), whereas façade "FC" uses steel lintels over large openings, "FG" use timber lintels, and FB" and "FH" do not have lintels. The selected façades include variations in wall geometry, wall thickness and openings, and idealize the features of Dutch URM buildings, described in section 1.1.

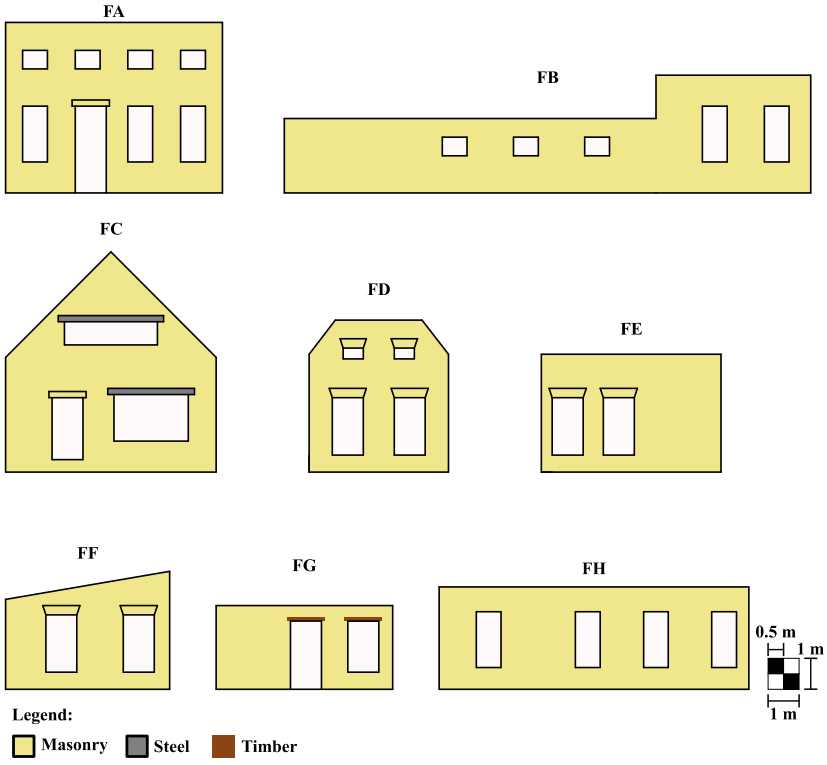

Fig. 4. The selected façades adopted in the numerical models. Each façade is associated with an ID, which is used to reference it. The dimensions of the façade are reported in Table 1, and further in detail in Ref. [49].

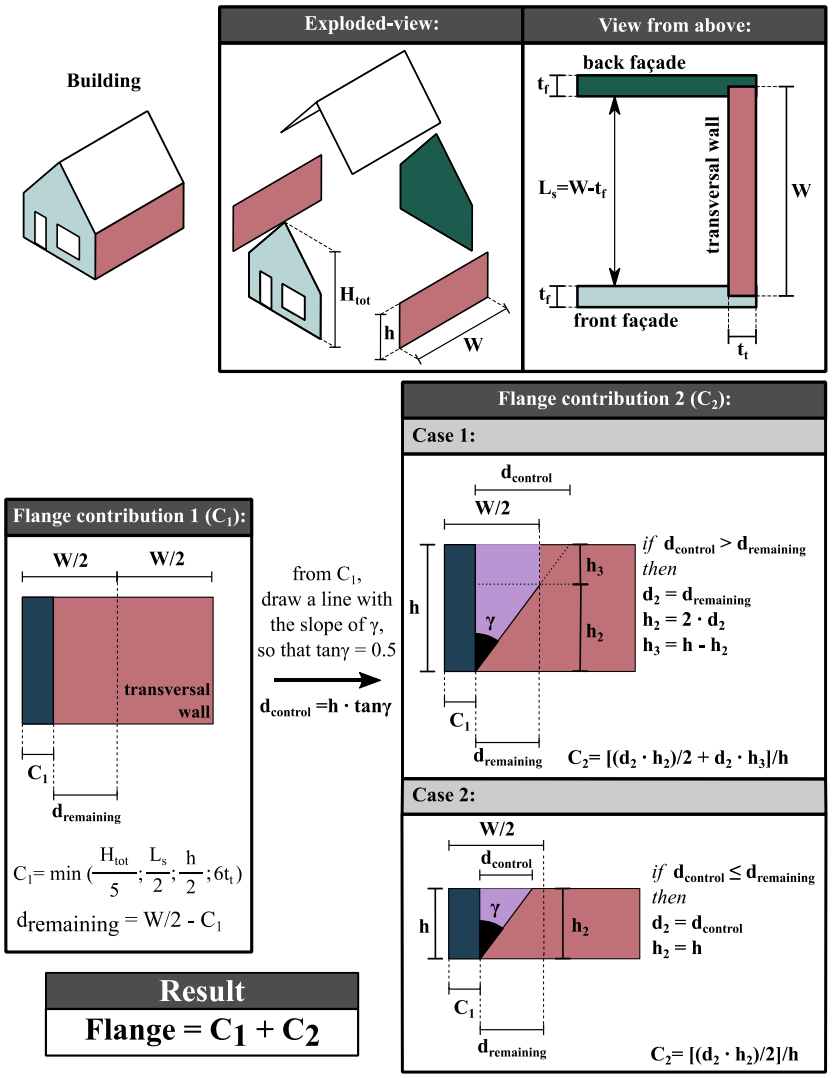

Fig. 5. The calculation of the effective flange width of the transversal walls adopted in the FE models. The parameter values are reported in Table 1.

Table 1
The geometrical parameters of the selected façades as shown in Fig. 4. The parameters "h", "t_t" and "W" refer to the transverse walls and the distance between the front and back façades, as shown in Fig. 5. The values are used to account for the effect of the transversal walls.

Parameter	Symbol	Units	Façade							
			FA	FB	FC	FD	FE	FF	FG	FH
Length	L	m	7.00	17.00	6.80	4.50	5.80	5.30	5.70	10.00
Height	H	m	5.50	3.80	7.10	4.90	3.80	3.80	2.70	3.30
Length over Height ratio	L/H	–	1.27	4.47	0.96	0.92	1.53	1.39	2.11	3.03
Façade thickness	t_f	m	0.21	0.21	0.10	0.21	0.21	0.21	0.21	0.10
Height of the Transversal Wall	h	m	3.80	2.40	3.00	3.80	3.80	2.90	2.70	3.30
Transversal Wall thickness	t_t	m	0.21	0.21	0.10	0.21	0.21	0.21	0.21	0.10
Distance between front and back façade	W	m	5.00	7.00	12.00	5.80	4.50	5.80	5.40	6.50
Opening ratio	$A_{openings}/A_{façade}$	–	0.21	0.09	0.21	0.20	0.17	0.21	0.11	0.17

2.2.2. *Modelling the effect of the transversal walls*

The models include the effect of the transverse walls in terms of stiffness and weight using the approach presented in Refs. [29,39]. Fig. 5 illustrates the parameters to be considered in the analytical formulation.

The Dutch standard [50] proposes a method to compute the length of the effective flange width as the sum of two areas: the normal

compressive force is provided by the part of the building wall located next to the cooperating flange width. The length of the cooperating flanges corresponds to the sum of two contributions (C_1, C_2 in Fig. 5).

- The first contribution ("C_1" in Fig. 5) considers the minimum of the following: i) a fifth of the building height ($H_{tot}/5$), ii) half of the internal distance between party walls ($L_s/2$) iii) half of the wall height ($h/2$) iv) six times the wall thickness ($6t_t$), as described in Ref. [51];
- The second contribution ("C_2" in Fig. 5), corresponds to the contribution to the normal compression given by the flange, as described in Ref. [50]. Two cases are distinguished for this calculation, based on the geometry of the transversal wall;

The parameters shown in Fig. 5 correspond to those of the selected façades reported in Table 1. The computed values of the cooperating flanges are used to model both the transversal walls and the transversal foundations.

2.2.3. Selected strip foundation systems

Two strip foundation systems are selected to represent common pre-1970 Dutch buildings.

- A URM foundation (Fig. 6a);
- A reinforced concrete (RC) strip below a masonry beam (Fig. 6b). The portion of masonry represents an extension of the wall which lies above the ground surface.

Regarding the RC foundation, the non-linear behaviour of the concrete material is included. Therefore, the longitudinal (i.e., along the façade) rebar system of the RC foundation is modelled as line reinforcement and considered fully embedded in the concrete with no slipping behaviour. The cross-section of the rebar is set to represent 4Ø16 both at the top and bottom. The URM foundations also take into account the material non-linearity.

2.2.4. Constitutive models and material properties

The non-linear cracking behaviour of the masonry material is modelled employing an orthotropic, smeared crack/slip/crush constitutive law, i.e., the Engineering Masonry Model (EMM) [52,53]. The EMM is a pre-fixed orthotropic model with total-strain-based stress-strain relations along the bed- and head-joint directions, including shear friction along bed-joints and the indirect inclusion of stepped diagonal cracking. The model incorporates both horizontal and vertical tensile and compressive softening, as well as shear softening. Unloading is modelled as secant for tension and elastic for shear. Unlike a rotating total-strain model, the crack orientations are pre-fixed [28].

The parameters in Table 2 correspond to the material properties of the clay brick masonry, based on laboratory tests and values from national guidelines [5,47,52,54,55]. Three material property sets are used that correspond to a "Standard" material, a "Weak"

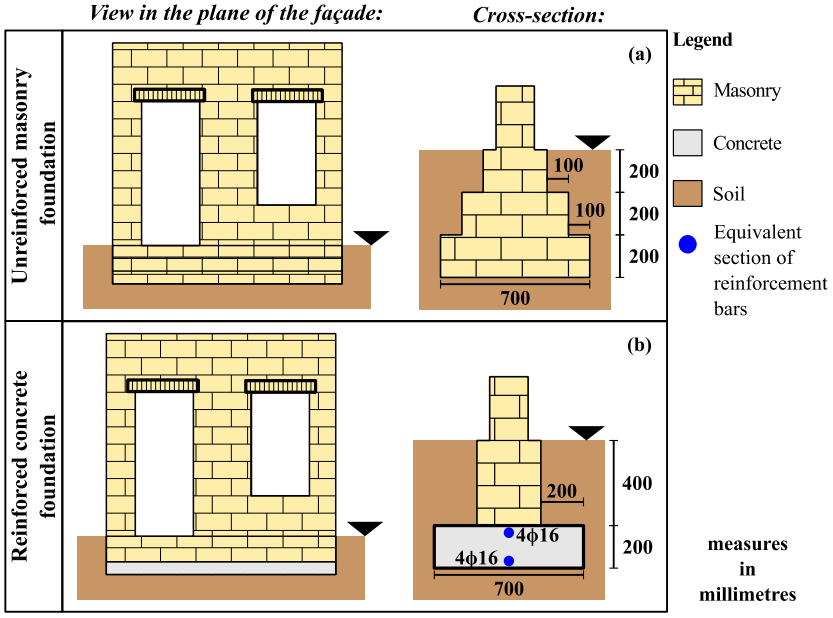

Fig. 6. The strip foundation system adopted in the numerical models: (a) URM foundation and (b) RC foundation. In the NLFEA, the soil volume is not modelled explicitly, and it is represented in the image to illustrate the intended depth of the foundation.

material, in which the properties of the standard material are reduced, and a "Strong" material, in which the properties are increased.

The EMM is adopted for the façade, the lintels and the URM foundation. The head-joint failure (representing vertical cracking) is based on friction, so a higher vertical pre-compression increases the head-joint strength. The minimum head-joint strength (when no pre-compression is present) is set to 1.5 times the bed-joint tensile strength [1,2]. To achieve mesh-size objectivity, the fracture energies are distributed over a crack band, which is related to the finite element size. In particular, crack bandwidth is determined by Govindjee's projection method [40].

For the lateral elements placed at the side of the façades to simulate the effect of the transversal walls, the Total Strain Rotating Crack model (TSRCM) [40] is adopted for the masonry material, as the EMM was not available for beam elements in the applied software. The Poisson's ratio is set to 0.25 so that the shear modulus G matches that of the EMM material. The TSRCM maintains the mass density of the EMM, while the tensile strength f_t values correspond to the f_{ty} values specified for the EMM in Table 2.

For the variations with the RC foundation, the non-linearity of concrete is modelled with the TSRCM [40]. The Von Mises Plasticity model [40] is employed for the steel material of the rebar in the RC foundations. A summary of such material properties is shown in Table 3. The steel used for the rebars in the case of RC foundations has Young's modulus equal to 210 GPa and yield stress equal to 235 MPa.

Both the steel and timber materials adopted for the lintels are modelled using linear elasticity. The timber has Young's modulus equal to 11000 MPa, Poisson's ratio equal to 0.35 and a mass density equal to 450 kg/m^3. The steel material used for the lintel has Young's modulus equal to 61204 MPa, Poisson's ratio equal to 0.35 and a mass density equal to 1120 kg/m^3. The properties of the steel material for the lintel have been chosen to ensure that the equivalent bending stiffness "EI" modelled as a rectangular section in the model corresponds to the "EI" of a steel beam with an IPE200 section.

Two soil materials are considered in the analyses, and are used in the following for the soil-structure interfaces (Coulomb-friction model [40]).

- Sand, characterized by a shear modulus G of 35 MPa, the Poisson's ratio equal to 0.3 and a friction angle of 30°;
- Clay, characterized by a shear modulus G of 10 MPa, the Poisson's ratio equal to 0.45 and a friction angle of 15°;

2.2.5. Boundary conditions, bedding and soil-foundation interaction

At the bottom of the strip foundation, interfaces are used to model the soil-foundation interaction, using a semi-coupled approach [17,21,22]. Two corner springs located beneath the transverse walls are used to model the soil-structure interaction for the transverse walls. Vertical and horizontal supports are prescribed at the bottom of the interface elements.

The interface uses the no-tension Coulomb-friction behaviour [40], whereas the values of the vertical and horizontal stiffness are determined for each soil material with the formulation reported in equations (2) and (3) [56,57] and already adopted in Refs. [21,29,38,39]. The dilatancy angle is also set to zero, and the friction angle is defined to match that of the corresponding soil scenario.

$$K_n = \frac{GL}{1-\upsilon}\left[0.73 + 1.54\left(\frac{B}{L}\right)^{0.75}\right] \tag{2}$$

$$K_t = GL\left\{\frac{1}{2-\upsilon}\left[2 + 2.5\left(\frac{B}{L}\right)^{0.85}\right] - \frac{0.2}{2(0.75-\upsilon)}\left[1 - \frac{B}{L}\right]\right\} \tag{3}$$

Where K_n, and K_t from equations (2) and (3) represent the normal and tangential (i.e., in the plane of the façade) directions to the soil surface. "B" represents the width of the base of the foundation, while "L" is the foundation length (equal to the length of the façade). "G" and "υ" are the shear modulus and the Poisson's ratio of the soil material. The values of K_n, and K_t are then divided by "B" and "L" to obtain smeared values of the normal and shear stiffness. For instance, the final smeared values for the façade "FA" on the clay soil are equal to 0.026 and 0.017 N/mm^3 for the normal and shear stiffness, respectively.

Table 2
Material properties adopted in the FE models.

Material Properties	Symbol	Unit of measure	Weak	Standard	Strong
Young's modulus vertical direction	E_y	MPa	2500	5000	7500
Young's modulus horizontal direction	E_x	MPa	1250	2500	3750
Shear Modulus	G_{xy}	MPa	1000	2000	3000
Bed-joint tensile strength	f_{ty}	MPa	0.050	0.100	0.150
Minimum strength head-joint	$f_{tx,\ min}$	MPa	0.075	0.150	0.225
Fracture energy in tension	$G_{f,I}$	N/m	2.6	10.0	22.4
Angle between stepped crack and bed-joint	α	rad	0.5	0.5	0.5
Compressive strength	f_c	MPa	4.25	8.50	12.75
Fracture energy in compression	G_c	N/mm	16.76	18.39	19.90
Friction angle	φ	rad	0.64	0.64	0.64
Cohesion	c	MPa	0.075	0.150	0.225
Fracture energy in shear	G_s	N/mm	0.025	0.100	0.224
Mass Density	ρ	Kg/m^3	1900	1900	1900

Table 3
Adopted material properties for the RC in the numerical models.

Material Properties	Symbol	Unit of measure	Concrete
Young's modulus	E	MPa	32000
Poisson's ratio	ν	–	0.2
Fracture energy in tension	$G_{f,I}$	N/mm	0.137
Compressive strength	f_c	MPa	33
Tensile strength	f_t	MPa	2.565
Mass density	ρ	Kg/m^3	2350

2.3. Interface between the masonry façade and the steel lintels

Coulomb-friction interfaces with gapping are used to simulate the contact behaviour between the masonry façade and steel lintel. The normal and tangential stiffness values, i.e., $k_{n,steel-masonry}$ and $k_{t,steel-masonry}$, of the lintel-masonry interface are computed using the equation reported in equations (4) and (5) reported in Refs. [58,59]:

$$k_{n,steel-masonry} = \frac{E_{steel}E_{y,masonry}}{h_m\left(E_{steel} - E_{y,masonry}\right)} \tag{4}$$

$$k_{t,steel-masonry} = \frac{G_{steel}G_{y,masonry}}{h_m\left(G_{steel} - G_{y,masonry}\right)} \tag{5}$$

E_{steel} and $E_{masonry}$ in equations (4) and (5) represent Young's moduli of the steel and the masonry material respectively, whereas G_{steel} and $G_{masonry}$ are the shear moduli. "h_m" represents the thickness of the mortar, assumed to be equal to 10 mm. The normal and shear stiffness values, for the "Standard" masonry material, computed with equations (4) and (5) are equal to 544 and 218 N/mm^3 respectively. The adopted friction angle is equal to 16.7° and the dilatancy angle is 0° whereas the cohesion and the tensile strength are equal to those of the masonry materials.

2.3.1. Finite element discretization

Plane stress elements with an average mesh size of 200 × 200 mm are used for the façade, foundation and lintels. Accordingly, 8-node quadratic quadrilateral elements with a 3 × 3 Gaussian integration scheme and 6-node quadratic triangular elements with 4 Gaussian points are used.

Class-III Mindlin beam elements are placed at the sides of the façade and foundation to model the transversal walls and foundations, following the approach implemented in Refs. [29,39].

The line interface elements use 3 + 3 node elements and the Newton-Cotes (5 points) integration scheme. The corner interfaces make use of 1 + 1 nodal interface elements.

2.3.2. Applied loads and settlement patterns

Vertical loads are applied to include the weight of the roof, floors and veneer (in the case of cavity walls for façade "FC" and "FH") as illustrated schematically in Fig. 7, whereas the values of each load for each façade are reported in Table 4.

Settlement troughs representing greenfield settlements, i.e., displacements caused by subsidence drivers in the absence of structures, are imposed as vertical displacements at the soil-foundation interface. This semi-coupled approach is consistent with previous studies [21,29,39,60].

Prior research [61] has demonstrated that the magnitude of horizontal ground displacements, quantified by horizontal strains, is highly relevant in cases of excavations, tunnelling, or mining works. However, for other subsidence drivers, horizontal strains may be

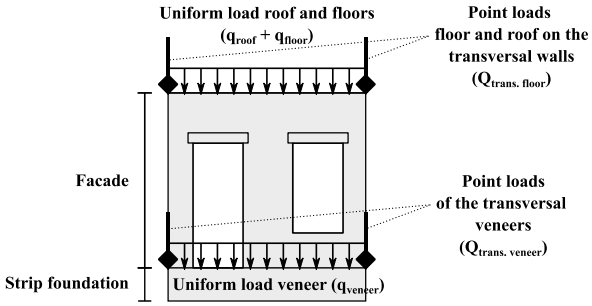

Fig. 7. Schematic illustration of the location and types of loads applied to the selected façades.

Table 4
The loads adopted in the finite element analyses of each façade, according to the loading scheme shown in Fig. 7.

Façade	Distributed loads			Point loads			
	q_{floor}	q_{roof}	q_{veneer}	$Q_{trans.\ floor,\ left}$	$Q_{trans.\ floor,\ right}$	$Q_{trans.\ veneer,\ left}$	$Q_{trans.\ veneer,\ right}$
	kN/m			kN			
FA	0	0	0	8.86	8.86	0	0
FB	0.62	4.46	0	0	16.50	0	0
FC	0	1.77	7.91	7.53	7.53	7.55	7.55
FD	0	0.41	0	5.50	5.50	0	0
FE	0	2.85	0	5.43	5.43	0	0
FF	0	0	0	4.19	9.42	0	0
FG	0	4.19	0	2.89	2.89	0	0
FH	0	5.33	5.08	0	0	8.76	8.76

smaller and are neglected in this study. Therefore, the approach adopted here better reflects situations with negligible horizontal strains, as may occur with shallow subsidence drivers unrelated to human activities. The imposed displacements conformed to a Gaussian curve are computed using equation (6) [62]. Prior research has demonstrated that Gaussian shapes can also be effectively used to represent building settlements caused by subsidence mechanisms other than tunneling, excavation, or mining [30,63,64].

$$S(x) = (-1)^{\iota}\left\{ e^{\left[\frac{-(x-D_x)^2}{2x_i^2}\right]} \right\} \tag{6}$$

Where S(x) is the vertical displacement along the direction "x", parallel to the façade length. "D_x" is the horizontal distance between the symmetry axis of the Gaussian curve and the edge of the building; "x_i" is the distance from the symmetry axis of the curve to the point of inflexion. "ι" is a **binary** parameter, either 0 or 1, that enables controlling the convexity of the Gaussian curve. The influence of the parameters of equation (6) is shown in Fig. 8 for a building of unitary length. Arbitrarily defined intervals of D_x, x_i and ι are used to generate 72 settlement shapes shown in Figs. 9 and 10.

All the selected settlement patterns are generated ensuring that the maximum angular distortion β along the profile, i.e., the slope of the line connecting two points relative to the tilt of the building [15], is equal to 1/300 (3.33 ‰). This is achieved with the following

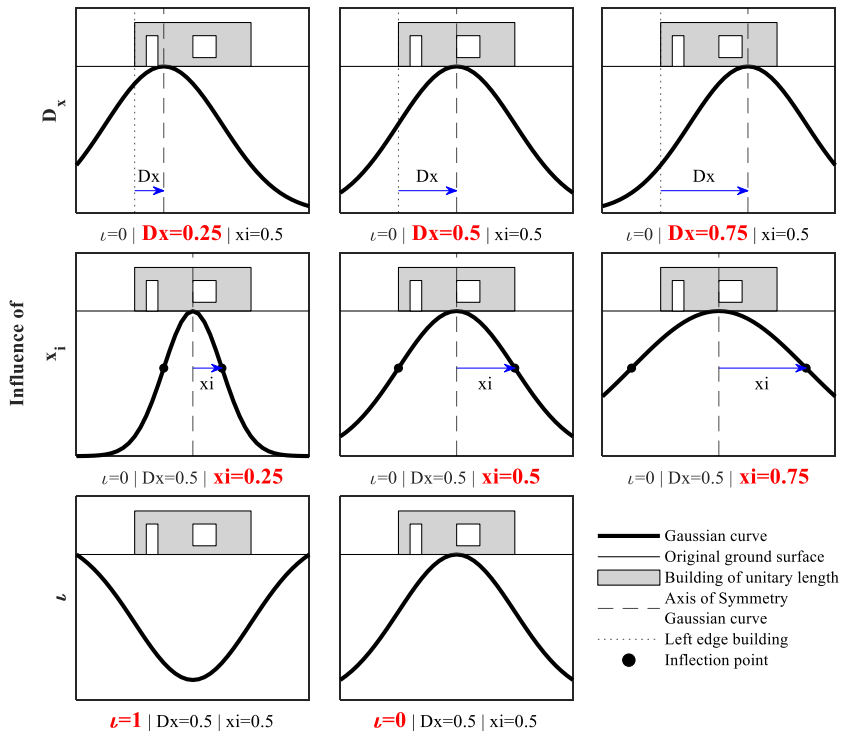

Fig. 8. Schematic illustration of the influence of the parameters in equation 6 used to generate the settlement shapes.

steps.

1. Equation (6) is used to generate the settlement deformation S(x) for a building of a unitary length (thus x ranges from 0 to 1). This step results in settlement shapes in Figs. 9 and 10 defined by two coordinates: the x-coordinate along the building and the z-coordinate representing vertical displacement.
2. The maximum value of S(x) is subtracted from all the z-coordinates, ensuring that S(x) values range between negative values and "0", which corresponds to the bottom edge of the foundation.
3. The x-coordinate values are scaled by the desired façade length L, transforming the unitary length into the actual building length (hence, x now ranges from 0 to L).
4. The maximum settlement of S(x) is set so that the maximum β along the profile is equal to 1/300 (3.33 ‰).

Figs. 9 and 10 illustrate that some of the shapes considered can be visually approximated by straight lines, where slope changes occur gradually (for instance, patterns with $x_i = 1.00$ and $D_x = -0.50$) while others exhibit more abrupt changes (e.g., symmetric sagging and hogging with x_i and D_x equal to 0.50). Settlement shapes that more closely resemble straight lines require a higher maximum settlement to achieve the target β.

The gravity, the vertical loads and the settlements are applied in the NLFEA using a two-step procedure.

1. Gravity and vertical loads (reported in Table 4) are applied separately with 10 steps each. After these 20 steps, the resulting displacement field of the façade was then cleared to keep track of the displacement field from the settlement loading only. The gravity and overburden loads are applied in multiple steps because it is possible that some non-linearities, and thus cracking, could occur already at this stage of the analyses.
2. Settlement profiles are applied as prescribed nodal displacements at the bottom of the soil-foundation interfaces. The number of steps used for the application of the settlements differs per shape (i.e., for each shape in Figs. 9 and 10). Each settlement pattern is applied progressively, increasing the displacement with a load step equal to 0.2 mm/step. In this way, the β was progressively increased from 0 (in the first step after the application of the gravity load) up to 1/300.

This research distinguishes between the "applied" settlements, which represent settlements in greenfield conditions, and the resulting displacements at the bottom of the façade, identified as "measured". Therefore, the distortion β imposed at the interface level is labelled as "applied β", whereas "measured β" is computed from the façade base displacements. Fig. 11 schematically illustrates the difference between applied and measured displacements.

2.3.3. *Direct and objective quantification of the damage*

For each step of the NLFEA during the settlement application, the resulting cracking damage is tracked. In this study, the parameter Ψ in equation (7) [28,42], is used to quantify the resulting progression and accumulation of the damage in the NLFEA in one single scalar value:

$$\Psi = 2\, n^{0.15}\, c_w{}^{0.3} \tag{7}$$

Where "n" is the number of cracks, "c_w" is the weighted crack width (in mm) calculated with equation (8):

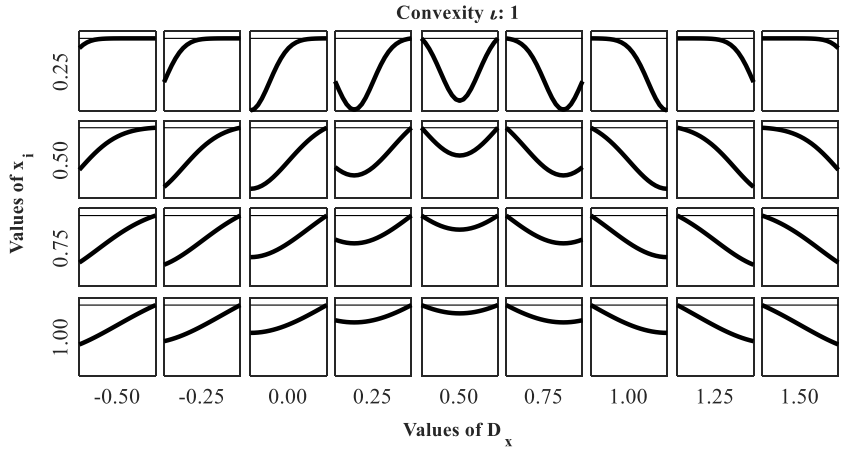

Fig. 9. The derived wide range of settlement shapes adopted in the numerical analyses based on selected intervals of the parameters D_x, x_i and for ι equal to 1.

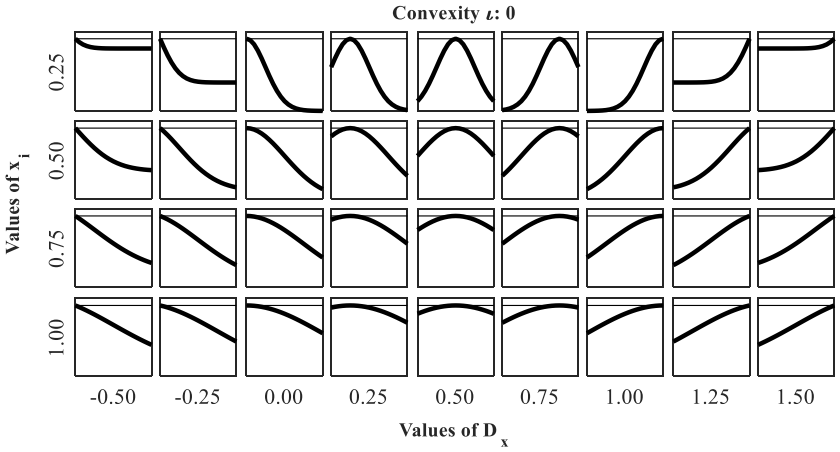

Fig. 10. The derived wide range of settlement shapes adopted in the numerical analyses based on selected intervals of the parameters D_x, x_i and for ι equal to 0.

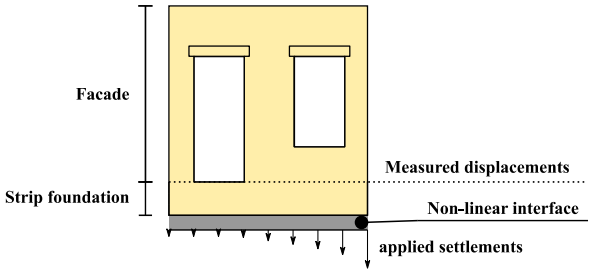

Fig. 11. Schematic illustration of the location of "applied" and "measured" displacements in the adopted NLFEA.

$$c_w = \frac{\sum_{i=1}^{n} {c_i}^2 L_i}{\sum_{i=1}^{n} c_i L_i} \tag{8}$$

$$c_i = \sqrt{{c_o}^2 + {c_s}^2} \tag{9}$$

Where "c_i" in equations (8) and (9) is the maximum crack width of crack "i" in millimetres, and "L_i" is the length in millimetres. The crack width is composed of both the opening (c_o) and sliding (c_s) components. The parameter Ψ was computed for the façades considering the output of the FE analyses, not including the foundation and the lateral beam elements.

A summary of the relation between Ψ and the approximate crack width for the various damage levels is presented in Table 5. Ψ is limited to the assessment of the light damage, i.e., up to cracks of about 5 mm wide, whereas damage that could affect the structural safety would require a different metric, possibly quantifying the reduction of the capacity of the structure.

3. Results

3.1. Computed damage Ψ for a selected model under increasing angular distortion β

This section illustrates an example of the results of the NLFEA, using the façade labelled as "FA", on the URM (as shown in Fig. 6a) on "Clay" soil, with "Standard" masonry material (Fig. 12). The reference analysis refers to one symmetric hogging settlement,

Table 5
Damage scale with the classification of visible damage and the corresponding discretization of Ψ (from Refs. [28,41,42,65]).

Damage level	Degree of damage	Approximate crack width	Parameter of damage
DL0	No Damage	Imperceptible cracks	$\Psi < 1$
DL1	Negligible	up to 0.1 mm	$1 \leq \Psi < 1.5$
DL2	Very slight	up to 1 mm	$1.5 \leq \Psi < 2.5$
DL3	Slight	up to 5 mm	$2.5 \leq \Psi < 3.5$
DL4	Moderate	5–15 mm	$\Psi \geq 3.5$

obtained with Dx = 0.5, xi = 0.5, ι = 0 (Fig. 10). Examples of different variations, including sagging, are shown in Ref. [49]. The maximum settlement is equal to about 8 mm to ensure the applied β is 1/300 applied to the model in 38 steps.

Fig. 13 illustrates the crack pattern during hogging settlement. Fig. 13a–d shows damage initiation and progression, while Fig. 13e summarises the relationship between applied β and the damage Ψ. Fig. 13f presents the relationship between applied β and measured β. In this analysis, cracks initially form around the corners of the openings. As the analysis progresses, a vertical crack develops from the top to the bottom of the façade, becoming the predominant crack, as symmetric hogging deformation induces tensile stresses at the top of the façade. When using the EMM, cracks predominantly develop in horizontal or vertical directions, while diagonal cracking occurs less frequently [21,66]. Nevertheless, this aspect is of limited concern in this study, diagonal cracks primarily form due to shear actions, which is not the dominant factor in this study.

The values of applied β vary between values ranging between 0 and 1/300 (Fig. 13e). This is not the case, however, for measured β (Fig. 13f). Instead, the measured β varies depending on the soil-structure interaction, material properties, geometry and damage level. Consequently, the maximum measured β varies among the different NLFEA.

The relationship between the maximum crack width and the damage parameter Ψ is shown in Fig. 14. The dashed line indicates the relationship between the maximum crack width and Ψ when only one crack is present. The differences from the theoretical trend can be explained by the presence of other smaller, diffuse cracks forming on the façade model, which are included in the calculation of Ψ.

Compared to relying on the maximum crack width, the advantage of using Ψ lies in its ability to condense cracking damage into a single parameter, enabling an objective quantification of its progression.

3.2. ECDF for each of the selected façade geometries

The applied and measured β are retrieved for discrete damage levels Ψ, ranging from 0.5 to 3.0 in increments of 0.5. The results of each façade are used to generate ECDF in Fig. 15, which express the ratio between the number of analyses that reach specific Ψ values for a given β, to the total number of analyses. For each façade, the ECDF show the results of 864 analyses, considering the selected combinations of 3 masonry materials, 2 soil materials, 2 foundation systems and 72 settlement shapes. The results of the façade are later grouped based on their L/H and presented in section 3.3.

The façade labelled as “FC” exhibits probabilities of damage higher than 0 before the application of settlement: This is attributed to its wide openings and single-wythe cross-section, which, in combination with the other features, result in damage caused by gravity loads (self-weight and overburden) before the settlement. These combinations implicitly simulate the effects of settlements on pre-damaged buildings. Some buildings may sustain pre-damage due to material degradation or actions other than settlements before settlement occurs, and the curves fictitiously account for this condition. It is worth noting that although the opening ratio (the ratio of the opening area to the wall area) for façade “FC” is similar to those of the other selected walls (ranging between 10 % and 20 % as indicated in Table 1), the width of the openings appears to play a critical role in the occurrence of damage due to gravity loads. However, since only “FC” includes wide openings, it is not possible to fully assess the impact of this factor.

The façades with the highest L/H ratios, namely “FB” and “FH,” exhibit the highest probabilities of damage at a given applied β. These façades are characterized by the highest L/H ratio values. Conversely, the “FD” façade, which has the smallest L/H ratio, exhibits the lowest probability of damage. The effect of the L/H ratio is discussed in detail in section 3.3.

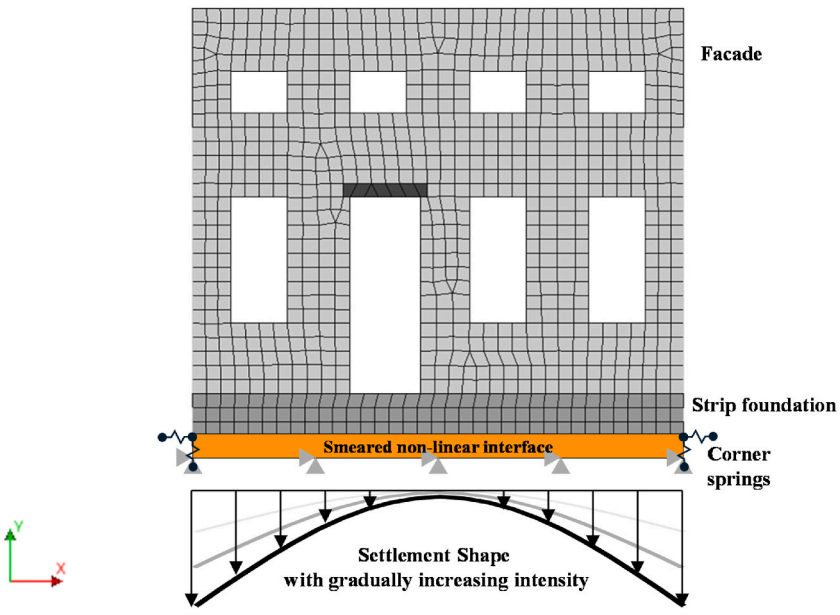

Fig. 12. Schematic illustration of façade labelled as “FA” with the URM foundation subjected to symmetric hogging.

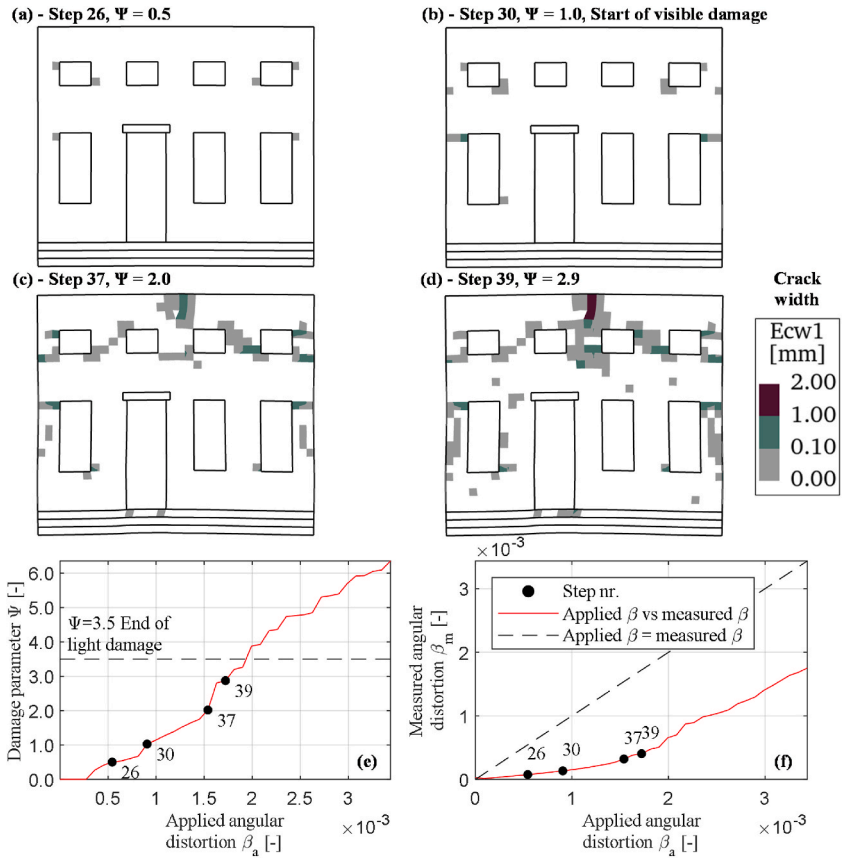

Fig. 13. Damage progression of the "FA" model under symmetric hogging (Dx = 0.5, xi = 0.5, ι = 0, see Fig. 10): from (a)–(d), contour plots display the maximum principal crack width (Ecw1) with deformation magnified by a factor of 50; (e) illustrates the relationship between applied β and the damage parameter Ψ, whereas (f) the relationship between applied and measured β. The markers (black dots) in (e) and (f) indicate various levels of Ψ, corresponding to each step in (a) through (d).

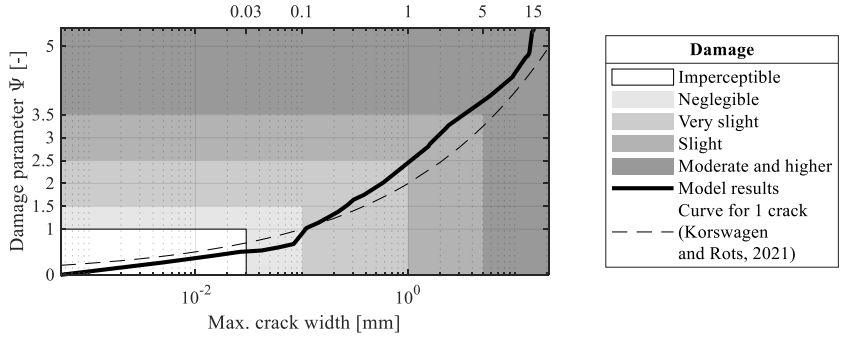

Fig. 14. Relationship between the maximum crack width against the damage parameter Ψ for the model "FA" subjected to symmetric hogging. The dashed line represents the trend for one crack [42]. The distinction of damage severity corresponds to the one in Table 5.

An interesting observation from the plots is the presence of an initial plateau in the curves for applied β below 0.25 ‰ (or 1/4000) before the distributions slope upward.

3.3. The influence of masonry and soil materials, façade length over height ratios, foundation systems, and settlement shapes

In this study, the extensive number of NLFEA allows for a separate examination of the effects of masonry materials, length-to-height (L/H) ratios, foundation systems, and soil types on the ECDF (Fig. 16). The variations in L/H ratios represent the grouping of results in Section 3.2, providing further insight into the influence of geometrical features. The influence of the different settlement shapes is

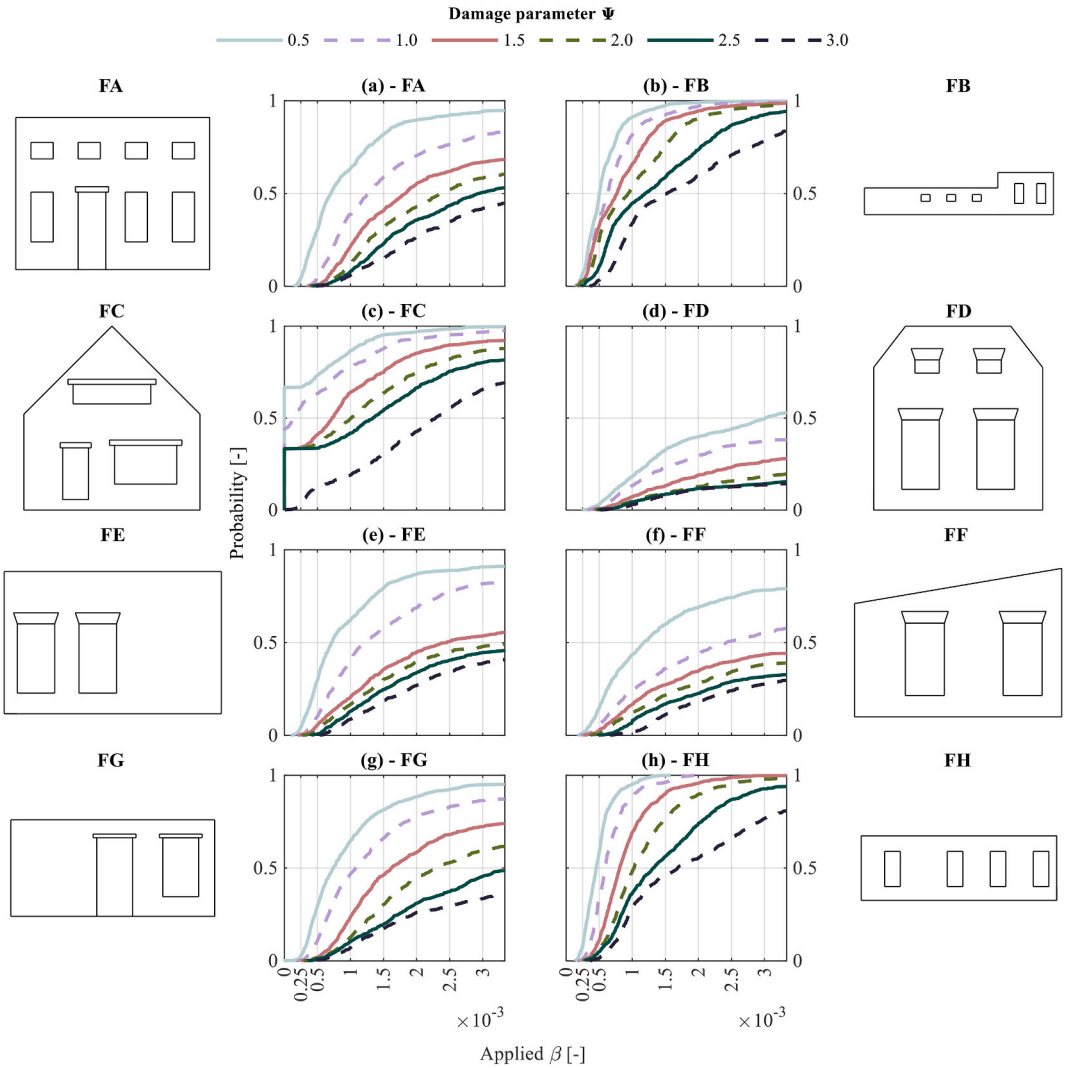

Fig. 15. The exceedance cumulative density functions (ECDF) for the selected eight façade geometries. The ECDF describe the probabilities of reaching specific levels of damage, expressed by Ψ values, as a function of the applied β.

shown in Fig. 17.

In Table 6, the probability of Ψ = 3.0 (crack width up to 5 mm) for increasing values of applied β is retrieved from the ECDF in Fig. 16. As expected, a stronger masonry material makes the models less vulnerable to the applied settlement (Fig. 16a). In slightly less than 40 % of the analyses, the "Strong" masonry does not even exhibit Ψ values higher than 1.0 (start of visible damage with a crack width up to 0.1 mm) at the end of the settlement application, which is represented by the area above the curve in Fig. 16a. This probability is equal to 20 % for "Standard" masonry, whereas almost all models with "Weak" masonry exhibit Ψ equal to 1.0.

For an applied β of 1/500 (2.00 ‰), the ECDF show that the probability of Ψ being equal to 3.0 almost doubles when transitioning from "Standard" to "Weak" masonry material. The difference is only 10 % when moving from "Strong" to "Standard" masonry.

In the models using the "Weak" masonry material, approximately 15 % show damage associated with a Ψ value of 2.0, indicating crack widths of 1 mm, before the application of settlements. This damage is therefore caused by gravity and overburden loads. However, this is not the case for the models with "Standard" and "Strong" masonry, highlighting the detrimental effect of weak masonry material on the models, jointly with specific geometries discussed previously.

The effect of the L/H ratios is shown in Fig. 16b. For the maximum value of applied β of 1/300, the façades with the smallest L/H (≤1.0) have the highest number of models that do not exhibit any significant damage (i.e., the part of the graph above the curve Ψ equal to 1.0), followed by L/H between 1.0 and 1.5, L/H between 1.5 and 2.5 and L/H higher than 2.5. Long façades are twice as vulnerable as short ones for specific values of the β. Specifically, with an applied β of 1/500 (2.00 ‰), façades with an L/H ratio of 2.5 or less show probabilities of Ψ being equal to 3.0 ranging from 20 % to 30 % (Table 6), while façades with an L/H ratio greater than 2.5 have twice that probability. It's important to note that this conclusion applies only to older buildings, which represent the focus of this study, as modern constructions typically include movement joints, which may allow buildings to accommodate settlements and reduce

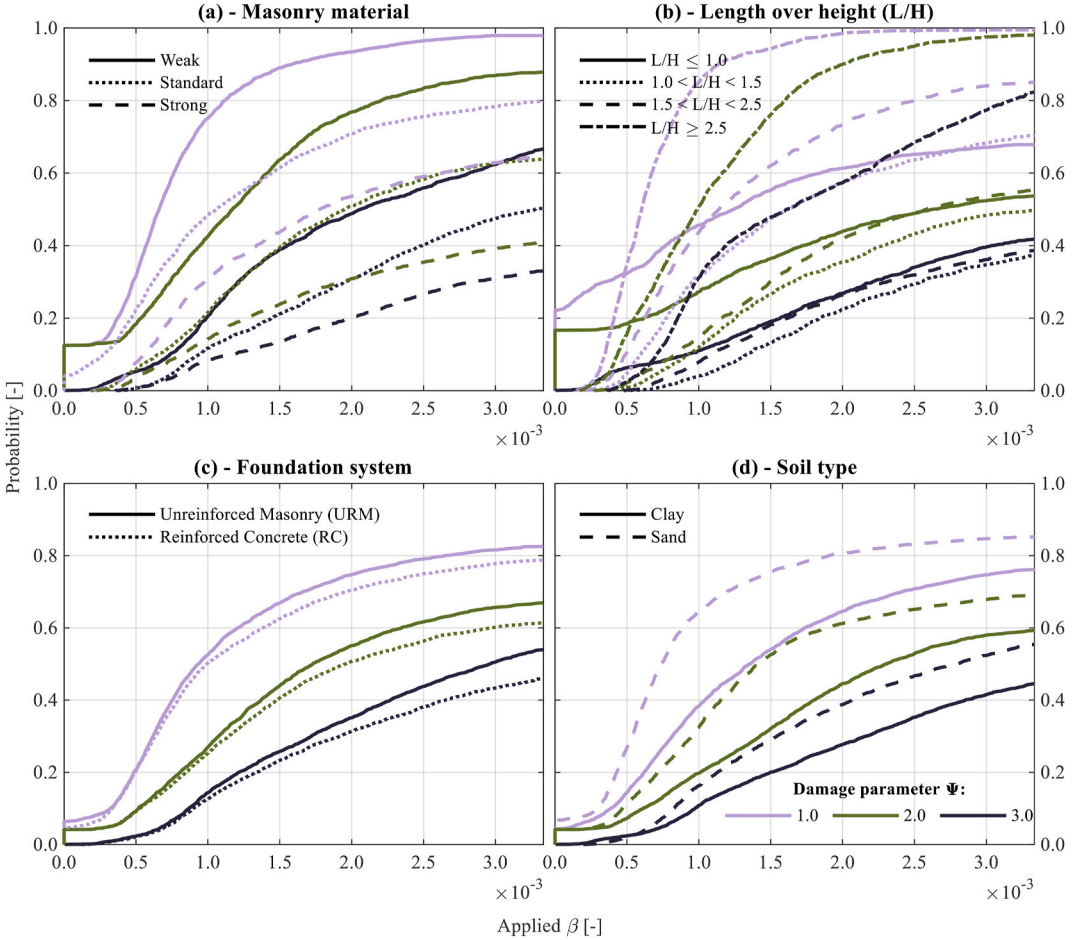

Fig. 16. Cumulative density functions in terms of applied β segregated by: (a) masonry material, (b) length over height ratio, (c) foundation system and (d) soil type.

the probability of cracking damage.

The effect of the selected foundation systems is shown in Fig. 16c. A notable observation is that for applied β below 1/2000 (0.50 ‰), the difference between RC and URM foundations is not significant. However, these differences become more pronounced at higher values of applied β, though they remain limited to no more than 10 %. In the selected RC foundation system, the distance between the top and bottom reinforcement bars is limited to the concrete section placed beneath the masonry enlargement. This limited distance between the rebar and the small concrete cross-section may not be sufficient to significantly increase the stiffness compared to URM foundations. The beneficial effect of reinforcement could be more pronounced in T-shaped RC concrete sections. However, these foundations are not included in this study, as they are more commonly found in more recent buildings, which fall outside the scope of this research. Furthermore, the reinforcement bars are expected to influence the model's response primarily in sagging settlement profiles, where concentrated tensile stresses occur at the bottom of the façade. In contrast, this beneficial effect diminishes during hogging conditions, where tensile stresses are concentrated at the top of the façade [49].

In Fig. 16d, the effect of the two selected soil materials is illustrated. Interestingly, the probability of damage for "Sand" is higher than that for "Clay". For example, at an applied β of 1/1000 (1.00 ‰) or higher, "Sand" soil reaches a probability of damage Ψ equal to 3.0 at approximately 16 %, while "Clay" only reaches 11 % (Table 6). Although this observation may seem counterintuitive, it can be explained physically by the ratio between the stiffness of the building and that of the soil: The selected soil properties influence the computed normal and tangential interface stiffness values at the bottom edge of the foundation system. In other words, changing the interface properties influences the ratio between the stiffness of the buildings and the soil-foundation interface. When "Clay" soil properties are used, the façade model acts relatively stiffer than in the case of the "Sand" soil; Thus, the models can better withstand the imposed distortions on clay soil rather than on sand. It should be noted, however, that in reality, high displacements due to shallow subsidence processes and, in turn, distortions, are more likely to occur in compressible soils, such as clay, rather than sands. Thus, although a stiffer interface, which results from sandy soil, represents the worst case for the numerical simulations herein presented, it is also unlikely that high values of distortions, such as those imposed herein in the analyses, would occur due to settlements.

The use of 72 settlement shapes reflects the variability of the different subsidence processes: depending on the settlement driver,

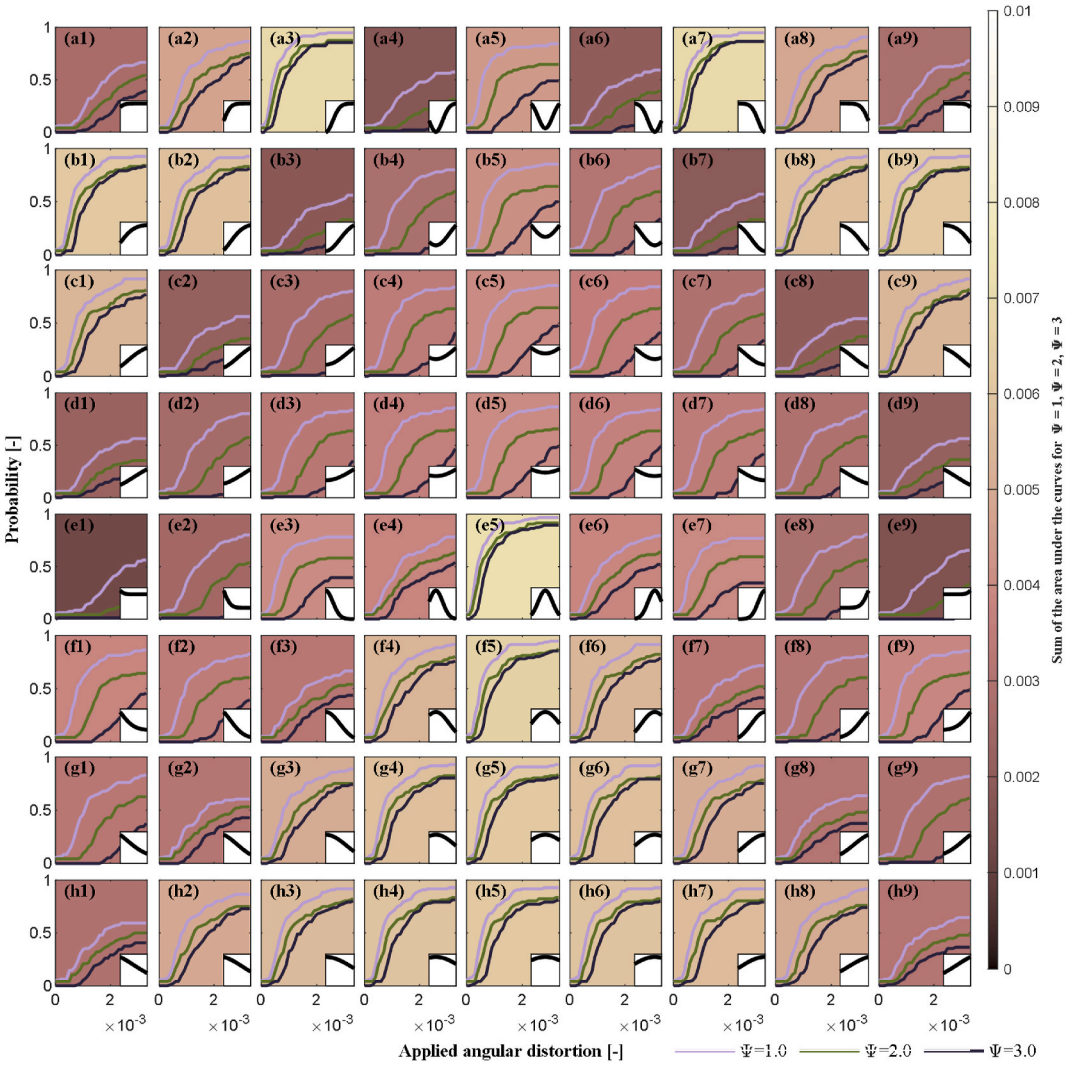

Fig. 17. Cumulative density functions in terms of applied β segregated by the different settlement shapes adopted in the NLEFA. The curves in terms of applied angular distortion against the probability of Ψ = 1.0, 2.0 and 3.0 are shown. The sum of the area under the three curves is used to distinguish the most detrimental settlement shapes, corresponding to the settlement shapes with the highest probability of damage causing damage. The colour scheme applied to the background of the plots reflects the sum of the area under the three curves. Light colours represent the most detrimental situations. The settlement shapes are also displayed on each plot, overlaid with the curves.

Table 6
Probabilities of damage for different values of applied β, distinguishing the selected modelling features. The values are retrieved from the distributions in Fig. 16.

Applied angular distortion β	Probability [%] of Ψ = 3.0 crack widths of up to 5 mm										
	Masonry			Length over Height L/H				Foundation		Soil	
	Weak	Standard	Strong	1.0 ≤ L/H	1.0 < L/H < 1.5	1.5 < L/H < 2.5	L/H ≥ 2.5	URM	RC	Clay	Sand
1/4000 (0.25 ‰)	1	0	0	2	0	0	0	0	0	1	0
1/2000 (0.50 ‰)	5	1	1	6	0	0	3	2	2	2	2
1/1000 (1.00 ‰)	21	12	8	11	4	8	32	15	13	11	16
1/500 (2.00 ‰)	49	31	20	26	22	26	58	35	31	28	39
1/300 (3.33 ‰)	66	50	33	42	38	39	82	54	46	45	56

different symmetric and asymmetric sagging and hogging shapes, ranging from pronounced to subtle curvature, can emerge and impact the buildings. Nevertheless, certain settlement shapes may have a more detrimental effect on a building, depending on their geometry. Fig. 17 presents the ECDF for Ψ = 1.0, 2.0, and 3.0 for each settlement shape used in the FE analyses. The sum of the areas

under the three curves serves as the metric to identify the most detrimental settlement shapes. Even if all the settlement shapes reach the maximum angular distortion β equal to 1/300, settlement shapes that more closely resemble straight lines require a higher maximum settlement to achieve the target β.

Settlement shapes characterized primarily by symmetric and asymmetric hogging exhibit the highest probability of damage and the most detrimental effects. In contrast, sagging settlement shapes, or those which resemble straight lines, have lower probabilities. Moreover, the distance between the curves for $\Psi = 1.0$, 2.0, and 3.0 indicates that damage progress more rapidly in hogging, rather than sagging. These observations align with the state-of-the-art [21,37,38,67,68].

Asymmetric settlement shapes can concentrate distortion in areas of the façade with a higher number of openings. The interplay between settlement shapes and geometry could, therefore, lead to increased stress on specific parts of the structure, potentially resulting in greater damage.

The 3 most and the 3 least detrimental settlement shapes for each façade are selected and shown in Fig. 18. The 3 most detrimental settlement shapes are the same for all the selected façades with the most severe being the symmetric hogging shape defined by $D_x = 0.5$, $x_i = 0.25$ and $\iota = 0$. The second and third most detrimental are asymmetric hogging shapes, flipped based on the façade, with the most damaging concentrating distortion beneath the area with the most openings, as seen in façades "FB", "FE", and "FG". In contrast, the least detrimental shapes and their ranking vary with façade geometry and correspond to sagging settlements or shapes with gradual slope changes, allowing the building to accommodate settlement without significant cracking.

In Fig. 19, box plots are used to represent the relative influence of the different selected parameters, with the median (black dot inside a white circle), the interquartile range (the bottom and top of each box correspond to the 25th and 75th percentiles of the sample, respectively), and the upper and lower bounds (whiskers) of the imposed β required to exhibit a Ψ value equal to 0.5. The plot focuses on the damage initiation stage (Ψ equal to 0.5), as not all models exhibit higher damage severity. The results are categorized according to the different parameters considered. The box plot for all the NLFEA is also shown, implicitly reflecting the influence of all the 72 settlement shapes.

An example of interpreting the plot can be seen in the "Weak" masonry material which has the lowest median and smallest interquartile range among all masonry types. This indicates that damage initiation occurs at lower applied β values compared to

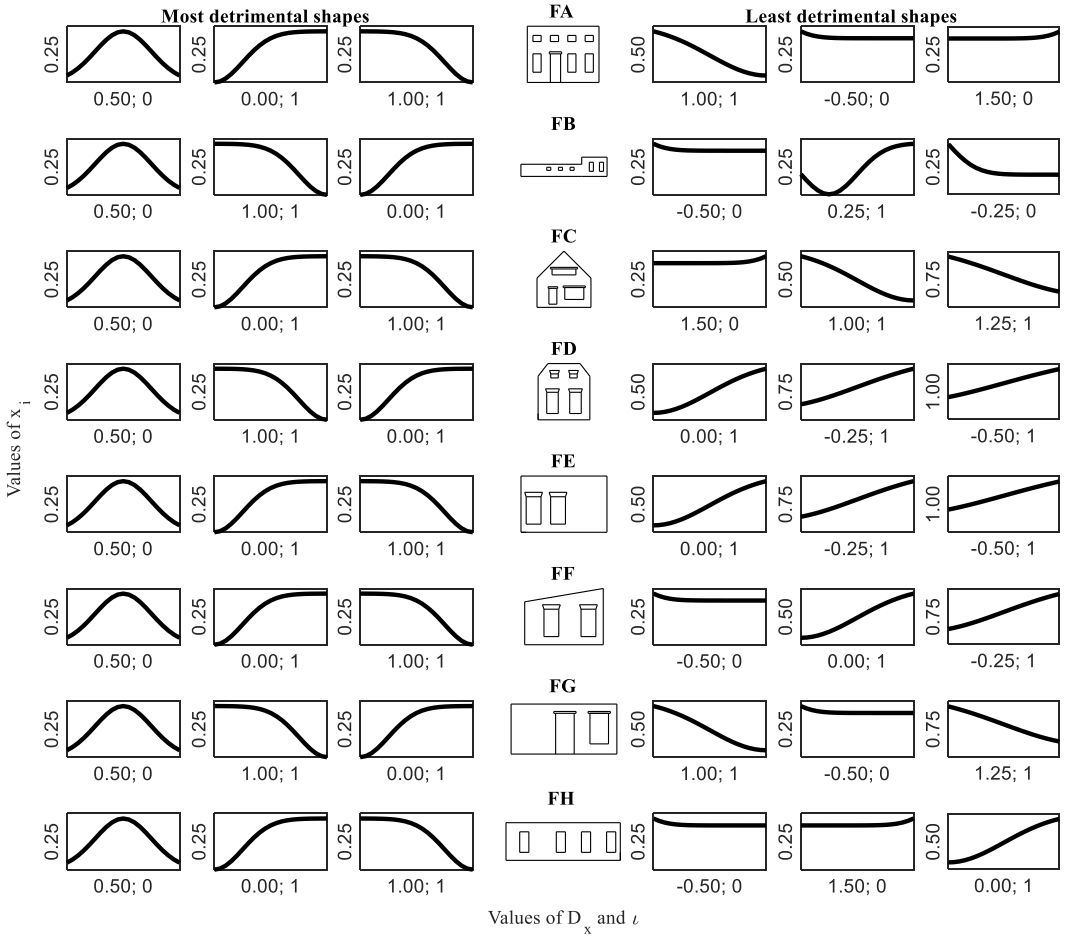

Fig. 18. The most and least detrimental settlement shapes for each selected façade are selected based on the results presented in Fig. 17.

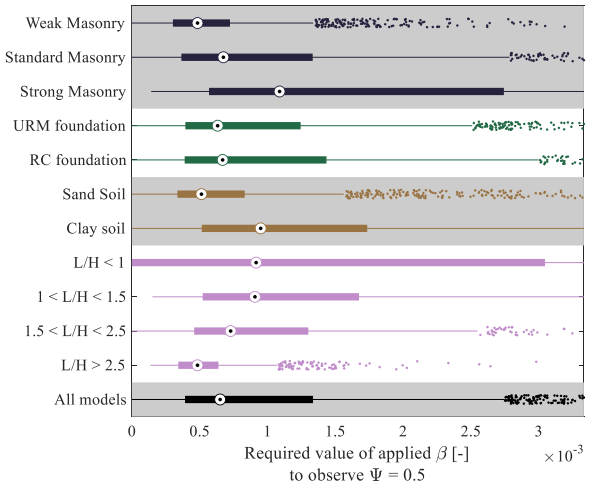

Fig. 19. Box plot of applied angular distortion for all the models at Ψ equal to 0.5, segregated by the different selected parameters. Each box plot shows the median of each subsample as a black dot inside a white circle, and the interquartile range as a thick bar. The lines that go from the interquartile range to the left and right of each box plot represent the whiskers, which extend to the most extreme data points not considered outliers. The whisker length is equal to 1.5 times the interquartile range. Outliers are represented as dots. A wide bar conveys a large variability.

"Standard" or "Strong" masonry. Additionally, the β values for "Weak" masonry show less variability, suggesting that model behaviour is strongly governed by its material properties. In contrast, as masonry strength increases with "Standard" and "Strong" materials, model behaviour becomes less dependent on masonry properties and more influenced by other model features. The spread of the box plots reveals that the most influential parameter is the L/H ratio, followed by the masonry material, and then the soil type, foundation, and settlement shape (indirectly shown in the box plot labelled as "All models"). The results align with the conclusions about the impact of building and soil features presented in Ref. [21].

4. NLFE-based fragility curves

The probabilities of damage to URM buildings undergoing subsidence are retrieved by NLFEA-based fragility curves (hereafter also referred to simply as "fragility curves"). First, the ECDF are retrieved considering the 6912 NLFEA, including the 8 selected façade geometries, the 3 masonry materials, the 2 shallow foundation systems, the 2 interface soil materials and the 72 settlement patterns ("ECDF" in Fig. 20).

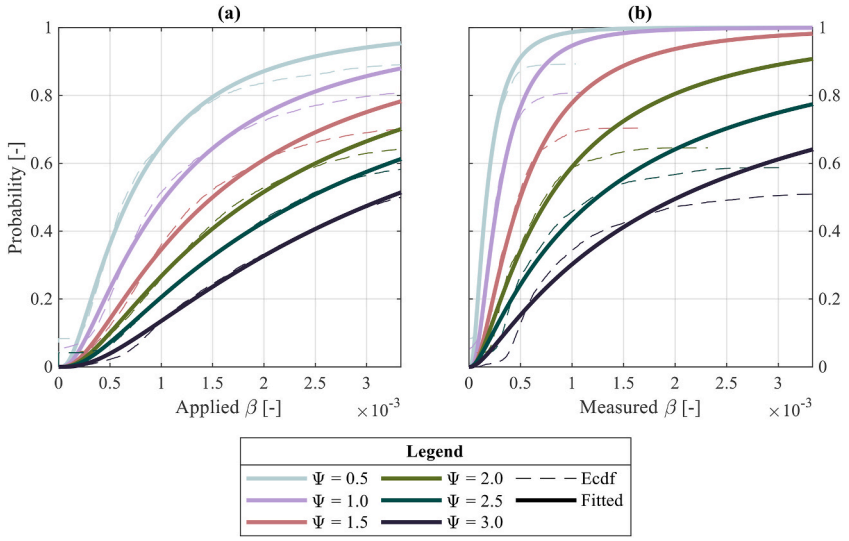

Fig. 20. The NLFE-based fragility curves in terms of applied (a) and measured (b) angular distortion considering the results of the 6912 analyses. "ECDF" represents the "exceedance" cumulative density functions, obtained by counting the number of models that reach a certain level of damage (expressed by the Ψ values) for a given angular distortion, to the total number of analyses.

As mentioned in section 3.2, the applied β varies between values ranging between 0 and 1/300 (Fig. 20a), whereas the maximum measured β does not have an upper bound as it depends on the soil-structure interaction, influenced by the model features. This results in the ECDF shown in Fig. 20b for different Ψ stopping at different values of measured β.

The ECDF were obtained considering all the analyses are fitted with equation (1) to generate the fragility curves shown in Fig. 20 ("Fitted"). Table 7 presents the parameters $\overline{SRI_i}$ and ζ_i of fragility curves for each Ψ value. The key advantage of fitting the ECDF is that once the parameters $\overline{SRI_i}$ and ζ_i are determined, the fragility curves can be readily reproduced for further studies using equation (1).

The Root Mean Squared Error (RMSE) serves as an indicator of how well the chosen log-normal function fits each ECDF. The RMSE values, expressed as absolute probability percentages, indicate the error around the fitted curves.

The fitted fragility curves begin at a probability of damage of zero (section 2), while the ECDF exhibit probabilities greater than zero even at no β, due to the pre-damage caused by gravity loads in the models of façade "FC" (see section 3.2). Overall, all the curves show a good fit for β values between 1/2000 (0.50 ‰) and 1/500 (2.00 ‰) with the differences increasing at higher β, leading to higher probabilities for the fitted curves. However, higher β values may induce damage exceeding light damage, not only in the form of cracking, which goes beyond the scope of this study.

The curves for applied β exhibit an initial plateau for values below 0.25 ‰ (or 1/4000), after which they begin to slope upward, resembling the distributions shown in Fig. 15. This plateau is absent in the curves for measured β (Fig. 20b).

Table 8 provides a summary of the probability values for the damage levels corresponding to different applied and measured β. Before the curves reach their plateau, it is notable that doubling β approximately doubles the probability of damage.

5. Discussion

5.1. Assumptions, limitations, and recommendations

In this study, two-dimensional NLFE models are used to investigate the response of structures undergoing subsidence, represented by two-dimensional settlement patterns. It is expected that three-dimensional settlement patterns may occur for existing structures, causing damage to certain exterior walls while leaving others undamaged. Consequently, the assumption that a single façade of the building can be used as a proxy for assessing the cracking damage of the entire structure is expected to yield conservative estimates. This approach assumes that the damage to the selected façade is representative of the damage to the entire building.

While this study primarily focuses on Dutch buildings, the findings and methodologies discussed have broad applicability to other regions facing similar challenges. Dutch buildings share many similarities with those in North America and parts of Europe, making the insights gained here relevant for addressing similar issues in these areas.

In the NLFEA, various combinations of material properties, foundation types, and soil conditions are considered. Some of these combinations are more representative of existing buildings than others. For example, the "Standard" masonry material is likely more prevalent in the building stock compared to the "Weak" or "Strong" variants. As a result, less common configurations with "Weak" or "Strong" masonry may have a greater influence on the fragility estimates than they would in a representative building stock. Conversely, more typical configurations may be underrepresented. While this approach allows for a broad exploration of structural behavior, it may lead to fragility curves that do not fully capture the actual distribution of vulnerabilities, and thus should be interpreted with this limitation in mind.

This observation supports the development of "weighted fragility curves", where model counts are adjusted using weights to reflect the probabilistic distribution of structural and geotechnical parameters observed in real buildings. However, the exact distribution and correlation of these features across the Dutch building stock remain largely unknown. Given this data gap, the study adopts a simplified modeling approach in which each combination of material properties, geometry, foundation type, and soil condition is assumed to have the same probability of occurrence. The absence of detailed probabilistic data constrains the application of more advanced uncertainty modeling techniques. Future work should aim to incorporate more refined uncertainty models as data availability improves, enabling a more rational and representative characterization of structural fragility.

In the NLFEA, the EMM has been used to model the non-linear cracking behaviour of the masonry material. The impact of using a smeared cracking approach to simulate settlement-induced damage in buildings has been examined in Ref. [11], where the EMM was shown to outperform other models in capturing damage severity when compared to experimental results. The EMM offers strong numerical stability and reliable convergence [66], a crucial factor given the extensive number of analyses conducted in this study. Despite its advantages, the model has limitations in damage localization, with cracks appearing as diffuse rather than sharply localized [52,66]. Nevertheless, such limitations are more relevant in the case of walls subjected to predominantly shear actions, which fall outside the focus of this study.

Regarding the modelling approach for soil-structure interaction, similar semi-coupled approaches have been used to reproduce the damage to existing structures [27,34]. The NLFEA exhibit measured deformations lower than the imposed greenfield ones, in line with the previous studies [21,69–71]. The NLFEA mainly focus on vertical soil displacements, whereas horizontal strains are not considered in the analysis. The horizontal strains play a significant role in human-induced subsidence, such as tunnelling, mining, and excavation, whereas this study examines subsidence triggered by other sources, including groundwater lowering, seasonal groundwater fluctuations, and peat oxidation. For these subsidence drivers, horizontal strains are expected to be significantly smaller, though further research is needed to confirm this aspect.

Thanks to the extensive number (6912) of analyses it was also possible to evaluate the influence of the different model features. Some combinations with façade "FC" exhibit cracks before the soil distortion is applied. This occurs due to the unfavourable combined

Table 7
Parameters fragility curves for applied and measured β values for the 6912 FE analyses.

Damage parameter Ψ	Applied β			Measured β		
	$\overline{SRI_i}$	ζ_i	RMSE	$\overline{SRI_i}$	ζ_i	RMSE
0.5	6.94E-04	0.93	2.30 %	1.70E-04	0.80	2.16 %
1.0	1.04E-03	0.99	2.55 %	2.85E-04	0.78	3.28 %
1.5	1.50E-03	1.02	2.34 %	5.00E-04	0.91	3.23 %
2.0	1.92E-03	1.05	1.74 %	7.81E-04	1.10	3.23 %
2.5	2.44E-03	1.09	1.30 %	1.25E-03	1.31	3.64 %
3.0	3.21E-03	1.06	1.62 %	2.03E-03	1.37	4.13 %

Table 8
Probabilities of different levels of damage based on the fragility curves proposed in Fig. 20.

Angular distortion β	Probability [%] for different values of the damage parameter											
	Fragility Curves for applied β						Fragility Curves for measured β					
	Ψ						Ψ					
	0.5	1.0	1.5	2.0	2.5	3.0	0.5	1.0	1.5	2.0	2.5	3.0
1/4000	14	8	4	3	2	1	69	43	22	15	11	6
1/2000	36	23	14	10	7	4	91	77	50	34	24	15
1/1000	65	48	35	27	21	14	99	95	78	59	43	30
1/500	87	74	61	52	43	33	100	99	94	80	64	50
1/300	95	88	78	70	61	51	100	100	98	91	77	64

effects of gravity load, overburden, and the wide openings, wall wythe, materials, and foundation systems, leading to cracking before subsidence occurs. However, analyses showing pre-settlement cracking could fictitiously represent pre-damaged buildings, where existing damage may result from shrinkage, previous settlement deformations, and thermal expansion, making walls more vulnerable to further damage.

The results of the analyses indicate that hogging settlement shapes are associated with a higher probability of damage compared to

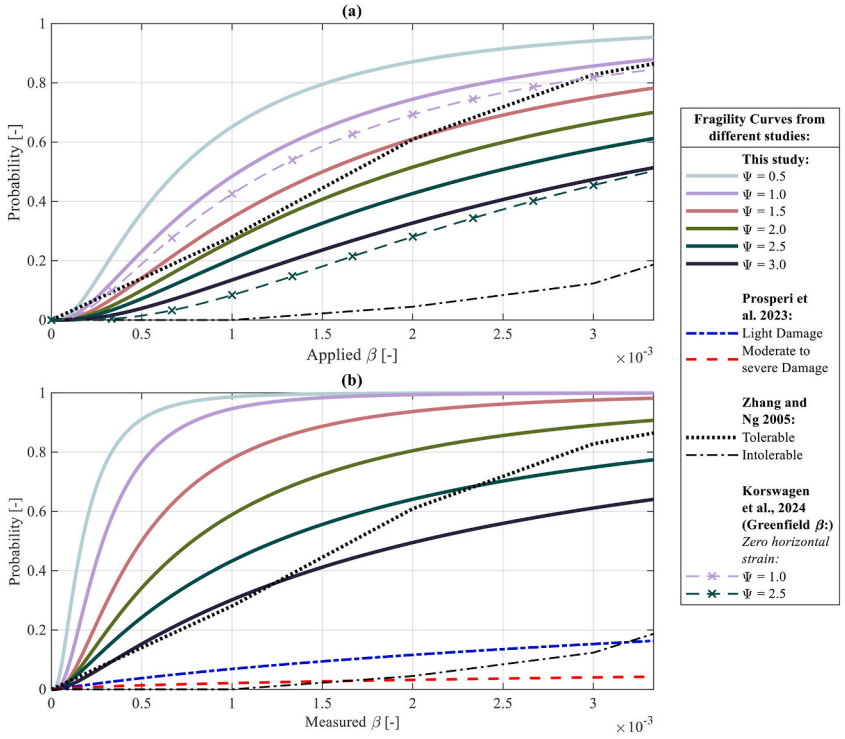

Fig. 21. Comparison of the proposed fragility curves in terms of (a) applied and (b) measured angular distortion β with the results of previous research.

sagging ones. Depending on the specific settlement shapes and the level of damage considered, the probability of damage can be up to twice as high for hogging. Moreover, damage progress more rapidly in the case of hogging compared to sagging. These observations align with the state-of-the-art [21,37,38,67,68]. Among the selected settlement shape, one symmetric hogging shape has been observed to be the most detrimental for the selected façades. However, the relationship between various settlement drivers, the resulting settlement and their shape still requires further investigation. It has been observed that the interaction between façade geometry and specific settlement shapes can create detrimental conditions, especially when distortion is concentrated in areas with more openings. Further analysis is recommended to evaluate how variations in wall geometry, including the number and distribution of openings, affect damage probability under different settlement shapes.

5.2. Comparison with prior research

Fig. 21 shows the comparison of the proposed fragility curves in terms of both applied and measured β with those from prior research. [72] investigates the combined effect of horizontal soil strains and angular distortions for URM buildings on shallow foundations, using 3D fully-coupled NLFEA in which the structure, the soil block and their non-linear behaviour and interaction are modelled; The study further develops fragility curves for various scenarios with different horizontal strain intensities. In Fig. 21a, the fragility curves by Ref. [72] without the effect of horizontal strains are compared with those proposed in this study, with discrepancies not exceeding 10 %.

The state-of-the-art literature offers several sets of fragility curves and ECDFs derived from empirical data. A dataset comprising a sample of 300 buildings was collected by Ref. [73], encompassing various structural typologies and construction materials, and further distinguishing buildings on shallow and deep foundations. The subset of buildings on shallow foundations, for which angular distortion data was available, includes 153 cases. The Authors classified cases as "tolerable" and "intolerable", without clarifying what damage these two terms refer to. According to other sources [36,74], "intolerable" cases refer to displacements and distortions affecting the functionality/safety and appearance of buildings. The "intolerable" curves have been compared to damage cases involving the complete damage of the structure, which may be economically or practically irreparable [74,75].

Due to the subjectiveness of the interpretation of the "tolerable" and "intolerable" curves, this study adopts a simplified approach by categorizing them as "light damage" (corresponding to $\Psi < 3.5$) and "moderate to severe damage" (corresponding to $\Psi > 3.5$). It is not clear if the distortion values reported were measured on the structures in all cases or inferred from soil data. Therefore, Fig. 21 shows the comparison with both applied and measured distortions computed from this study.

Overall, a good agreement is observed between the curves proposed in this study and the "tolerable" one by Ref. [73]. The curve of "intolerable" cases has a slower growth rate, which can be explained by the fact that it may refer to cases for which the equivalent Ψ would be way higher than 3.

The curves herein proposed in terms of measured β are compared with those obtained by Ref. [30] using measurements from existing buildings.

The differences between the different sets of curves are detailed in Table 9.

Compared to previous research, this study presents fragility curves that objectively differentiate between various levels of light damage. The proposed fragility curves can be used to estimate the probability of damage associated with different thresholds from established international guidelines and standards. For instance, in the Eurocode [67] it is reported that "*A maximum relative rotation of 1/500 is acceptable for many structures*". In this study, a measured β equal to 1/500 (2.00 ‰) corresponds to a probability of $\Psi = 3.0$ (cracks up to 5 mm) equal to 47 %. This implies that roughly one in every two buildings could exhibit damage requiring repointing or, in some cases, the replacement of bricks, depending on the quantity and location of cracks [41]. Nevertheless, at this damage intensity, such cracks in structural walls may remain without compromising the safety of the structure, granting some validity to the threshold proposed by the guidelines.

Table 9
Comparison of different aspects and limitations between empirical and numerical studies for structures affected by settlements.

Aspect	Empirical Observations	Numerical Models
Building Representation	Damage is measured on the entire building, which may be lower due to 3D effects.	Façade models are used as a proxy for the whole building, potentially overestimating damage.
Time-Dependency Effects	Settlement development and the visco-elastic response of masonry are time-dependent.	Time-dependent effects are not depicted in the model.
Sampling & Representativeness	Empirical datasets often consist of convenience samples (tens or hundreds of cases) that may not represent the entire population (millions of buildings).	Not applicable.
Inspection Bias	Inspections tend to target visibly damaged buildings, potentially overlooking cases with high distortion but no damage.	Not applicable.
Multiple Damage Drivers	Damage may be caused by several factors (e.g., thermal, chemical, accidental loads, storms) alongside settlement.	The analysis focuses solely on settlement-induced damage.
Material Properties Calibration	Small masonry samples may exhibit a more flexible behaviour than what is modelled.	Material properties have not been calibrated against large masonry samples.
Damage Classification	Damage classification is performed fuzzy, potentially increasing variability.	A more objective method is used for assessing damage.
Measurement Techniques	Measurements from real walls, taken at fixed intervals, may overestimate the distortion values at which damage appears.	Distortions are measured under controlled conditions in the numerical model.

6. Conclusions

In this study, 6912 non-linear finite element analyses (NLFEA) were carried out to develop fragility curves for unreinforced masonry buildings on shallow foundations subjected to subsidence-related settlements. The analyses include 8 variations of the façade geometry, 2 shallow foundations, 3 masonry materials, 2 soils, and 72 settlement shapes. While the study focuses on unreinforced baked clay masonry buildings constructed in the Netherlands before 1970, the proposed methodological approach is applicable to other regions and building typologies.

Two sets of fragility curves are proposed to support damage assessment over large areas.

- Fragility curves in terms of applied angular distortion are suitable for evaluating and predicting cracking damage to buildings when only the greenfield ground deformations are known, such as those obtained via modelling or regional remote surveying of the ground, such as InSAR.
- Fragility curves in terms of angular distortion measured on the building are intended for use in damage assessment procedures where the deformations of buildings are known.

The two sets of curves, focusing on "light damage", are compared with findings from previous research. Based on the analysis results, it has been observed that.

- For a value of the angular distortion measured on the building equal to 2 ‰ (or 1/500), the analyses indicated that 1 out of 2 façades might exhibit cracks up to 5 mm. This highlights the need for caution when using deterministic limit values, underscoring the importance of applying engineering judgment that considers the soil and structural features.
- For an applied angular distortion equal to 2 ‰ (1/500), the analyses show that long façades are twice as likely to experience 5 mm cracks from settlement damage compared to short ones.
- Before the fragility curves reach their plateau, doubling the imposed angular distortion approximately doubles the probability for all damage levels.
- Differences are observed between the results of models and empirical cases. This points toward the urgent necessity of experimental campaigns, empirical observation and monitoring data to validate and calibrate future numerical analyses.
- The analyses indicate that the L/H ratio is the most critical parameter influencing the structure's damage response for the considered sample of analyses, followed by masonry material, soil type, foundation, and settlement shape.
- For an applied angular distortion of 2 ‰ (1/500), the probability of experiencing cracks up to 5 mm almost doubles when transitioning from "Standard" to "Weak" masonry.
- Models with reinforced concrete foundations showed a lower probability of damage (10 % less) compared to those on unreinforced masonry foundations.
- Specific combinations of settlement shapes and façade geometry can increase the probability of damage. This entails settlement profiles that concentrate the distortion in vulnerable areas of the building, such as sections of the façade with more openings.
- Preventing light damage in existing structures due to subsidence may not be feasible. Even with applied angular distortions as low as 0.5 ‰ (or 1/2000), cracking damage occurs in approximately 10 % of cases, with cracks up to 1 mm wide.

CRediT authorship contribution statement

Alfonso Prosperi: Writing – review & editing, Writing – original draft, Visualization, Software, Methodology, Investigation, Formal analysis, Data curation, Conceptualization. **Paul A. Korswagen:** Writing – review & editing, Supervision, Software, Methodology, Conceptualization. **Michele Longo:** Writing – review & editing, Supervision, Methodology, Investigation, Formal analysis, Data curation, Conceptualization. **Mandy Korff:** Writing – review & editing, Supervision, Funding acquisition, Conceptualization. **Jan G. Rots:** Writing – review & editing, Supervision, Funding acquisition, Conceptualization.

Data availability statement

The original contributions presented in the study are included in the article, further inquiries can be directed to the corresponding author.

Declaration of competing interest

The authors declare that they have no known competing financial interests or personal relationships that could have appeared to influence the work reported in this paper.

Acknowledgements

The research presented in this paper is part of the project Living on Soft Soils: Subsidence and Society (grantnr.: NWA.1160.18.259). This project is funded by the Dutch Research Council (NWO-NWA-ORC), Utrecht University, Wageningen University, Delft University of Technology, Ministry of Infrastructure & Water Management, Ministry of the Interior & Kingdom Relations,

Deltares, Wageningen Environmental Research, TNO-Geological Survey of The Netherlands, STOWA, Water Authority: Hoogheemraadschap de Stichtse Rijnlanden, Water Authority: Drents Overijsselse Delta, Province of Utrecht, Province of Zuid-Holland, Municipality of Gouda, Platform Soft Soil, Sweco, Tauw BV, NAM.

Data availability

No data was used for the research described in the article.

References

[1] P. Korswagen, M. Longo, J. Rots, A. Prosperi, Supporting Analyses to Determine Probability of Damage and Fragility Curves due to Indirect Subsidence Effects, Delft University of Technology, October 3, 2022.
[2] P. Korswagen, M. Longo, J. Rots, A. Prosperi, Appendixes to Supporting Analyses to Determine Probability of Damage and Fragility Curves due to Indirect Subsidence Effects, Delft University of Technology, 2022. Report.
[3] Kadaster. Praktijkhandleiding Bag - Handleiding Bij De Catalogus Van De Basisregistratie Adressen En Gebouwen.
[4] H.U. Crowley, Scheefhals Jeroen, Roy, Exposure database (EDB) V7 - data documentation technical report and exposure model, ARUP (2020).
[5] S. Jafari, Material Characterisation of Existing Masonry: a Strategy to Determine Strength, Stiffness and Toughness Properties for Structural Analysis, Delft University of Technology: TU Delft Applied Mechanics, 2021. https://repositorytudelftnlDoctoralthesis.
[6] F. Messali, R. Esposito, S. Jafari, G. Ravenshorst, P. Korswagen, J.G. Rots, A multiscale experimental characterisation of Dutch unreinforced masonry buildings, 16th European conference on earthquake engineering (2018). Thessaloniki.
[7] R. Peters, B. Dukai, S. Vitalis, J. van Liempt, J. Stoter, Automated 3D reconstruction of LoD2 and LoD1 models for all 10 million buildings of the Netherlands, Photogramm. Eng. Rem. Sens. 88 (2022) 165–170.
[8] 3DBAG - data sources. https://docs.3dbag.nl/en/overview/sources/.
[9] The Council for the Environment and Infrastructure (Rli), Goed Gefundeerd: Advies Om Te Komen Tot Een Nationale Aanpak Funderingsproblematiek, 2024.
[10] P.A. Korswagen, M. Longo, A. Prosperi, J.G. Rots, K.C. Terwel, Modelling of damage in historical masonry façades subjected to a combination of ground settlement and vibrations. International Conference on Structural Analysis of Historical Constructions, Springer, 2023, pp. 904–917.
[11] A. Prosperi, M. Longo, P.A. Korswagen, G. Giardina, J.G. Rots, Comparative study of NLFE models for simulating settlement-induced damage in masonry façades: macro-and simplified micro-models, Frontiers in Built Environment 11 (2025) 1618329.
[12] A.W. Skempton, D.H. MacDonald, The Allowable Settlements of Buildings, vol. 5, Proceedings of the Institution of Civil Engineers, 1956, pp. 727–768.
[13] D.E. Polshin, R. Tokar, Maximum allowable non-uniform settlement of structures. Proc, 4th Int Conf on Soil Mechanics and Foundation Engineering, Butterworth's London, 1957, pp. 402–405.
[14] L. Bjerrum, Allowable settlement of structures. Proceedings of the 3rd European Conference on Soil, Mechanics and Foundation Engineering, Wiesbaden, 1963, pp. 135–137. Germany.
[15] J.B. Burland, C. Wroth, Settlement of Buildings and Associated Damage, 1975.
[16] M. Son, E.J. Cording, Estimation of building damage due to excavation-induced ground movements, J Geotech Geoenviron 131 (2005) 162–177.
[17] G. Giardina, A.V. Van de Graaf, M.A.N. Hendriks, J.G. Rots, A. Marini, Numerical analysis of a masonry facade subject to tunnelling-induced settlements, Eng. Struct. 54 (2013) 234–247.
[18] G. Giardina, A. Marini, M.A.N. Hendriks, J.G. Rots, F. Rizzardini, E. Giuriani, Experimental analysis of a masonry facade subject to tunnelling-induced settlement, Eng. Struct. 45 (2012) 421–434.
[19] G. Giardina, M.A.N. Hendriks, J.G. Rots, Sensitivity study on tunnelling induced damage to a masonry facade, Eng. Struct. 89 (2015) 111–129.
[20] Y. Liu, H. Burd, D.B. Gulen, K.D. Dalgic, B. Gilson, A. Ilki, et al., Estimation of settlement-induced damage in masonry buildings from displacement measurements, Tunn Undergr Sp Tech 157 (2025) 106314.
[21] A. Prosperi, M. Longo, P.A. Korswagen, M. Korff, J.G. Rots, Sensitivity modelling with objective damage assessment of unreinforced masonry facades undergoing different subsidence settlement patterns, Eng. Struct. 286 (2023) 116113.
[22] H.D. Netzel, Building Response due to Ground Movements, 2009.
[23] H. Burd, W. Yiu, S. Acikgoz, C. Martin, Soil-foundation interaction model for the assessment of tunnelling-induced damage to masonry buildings, Tunn Undergr Sp Tech 119 (2022) 104208.
[24] H.J. Burd, G.T. Houlsby, C.E. Augarde, G. Liu, Modelling tunnelling-induced settlement of masonry buildings, P I Civil Eng-Geotec 143 (2000) 17–29.
[25] W.N. Yiu, H.J. Burd, C.M. Martin, Finite-element modelling for the assessment of tunnel-induced damage to a masonry building, Geotechnique 67 (2017) 780–794.
[26] S. Ferlisi, G. Nicodemo, D. Peduto, Numerical Analysis of the Behaviour of Masonry Buildings Undergoing Differential Settlements, 2019.
[27] L. Bejarano-Urrego, E. Verstrynge, A. Drougkas, G. Giardina, M. Bassier, M. Vergauwen, et al., Numerical analysis of settlement-induced damage to a masonry church nave wall. Structural Analysis of Historical Constructions, Springer, 2019, pp. 853–861.
[28] P.A. Korswagen, Quantifying the Probability of Light Damage to Masonry Structures: an Exploration of Crack Initiation and Progression due to Seismic Vibrations on Masonry Buildings with Existing Damage, Delft University of Technology, 2024.
[29] A. Prosperi, M. Longo, P.A. Korswagen, M. Korff, J.G. Rots, 2D and 3D modelling strategies to reproduce the response of historical masonry buildings subjected to settlements, Int J Archit Herit (2024) 1–17.
[30] A. Prosperi, P.A. Korswagen, M. Korff, R. Schipper, J.G. Rots, Empirical fragility and ROC curves for masonry buildings subjected to settlements, J. Build. Eng. 68 (2023) 106094.
[31] K.D. Dalgic, B. Gulen, Y. Liu, S. Acikgoz, H. Burd, M. Marasli, et al., Masonry buildings subjected to settlements: Half-scale testing, detailed measurements, and insights into behaviour, Eng. Struct. 278 (2023) 115233.
[32] J. Ninić, A. Gamra, B. Ghiassi, Real-time assessment of tunnelling-induced damage to structures within the building information modelling framework, Undergr. Space 14 (2024) 99–117.
[33] E. Bilotta, Soil-structure interaction in tunnel construction in soft ground, Italian Geotechnical Journal-Rivista Italiana Di Geotecnica 51 (2017) 5–30.
[34] A. Drougkas, E. Verstrynge, P. Szekér, G. Heirman, L.-E. Bejarano-Urrego, G. Giardina, et al., Numerical modeling of a church nave Wall subjected to differential settlements: Soil-structure interaction, time-dependence and sensitivity analysis, Int J Archit Herit 14 (2019) 1221–1238.
[35] S. Ferlisi, G. Nicodemo, D. Peduto, C. Negulescu, G. Grandjean, Deterministic and probabilistic analyses of the 3D response of masonry buildings to imposed settlement troughs, Georisk 14 (2020) 260–279.
[36] D. Peduto, M. Korff, G. Nicodemo, A. Marchese, S. Ferlisi, Empirical fragility curves for settlement-affected buildings: analysis of different intensity parameters for seven hundred masonry buildings in the Netherlands, Soils Found. 59 (2019) 380–397.
[37] G. Giardina, J. Rots, M. Hendriks, Modelling of Settlement Induced Building Damage, 2013.
[38] A. Prosperi, M. Longo, P.A. Korswagen, M. Korff, J.G. Rots, Shape matters: influence of varying settlement profiles due to multicausal subsidence when modelling damage in a masonry façade, Tenth International Symposium on Land Subsidence 2023 (2023).
[39] A. Prosperi, M. Longo, P.A. Korswagen, M. Korff, J.G. Rots, Accurate and efficient 2D modelling of historical masonry buildings subjected to settlements in comparison to 3D approaches. International Conference on Structural Analysis of Historical Constructions, Springer, 2023, pp. 232–244.
[40] DIANA FEA bv, Finite Element Analysis User's Manual - Release 10.8. Laan Van Waalhaven 462, 2497 GR, the Hague, the Netherlands, 2024.

[41] J.B. Burland, B.B. Broms, V.F. De Mello, Behaviour of Foundations and Structures, 1978.
[42] P.A. Korswagen, M. Longo, E. Meulman, J.G. Rots, Crack initiation and propagation in unreinforced masonry specimens subjected to repeated in-plane loading during light damage, Bull. Earthq. Eng. 17 (2019) 4651–4687.
[43] A. Saeidi, O. Deck, T. Verdel, Development of building vulnerability functions in subsidence regions from empirical methods, Eng. Struct. 31 (2009) 2275–2286.
[44] A. Gurbuz, M. Tekin, Use of cumulative distribution functions in order to estimate damage probability, VFAST Transactions on Mathematics 7 (2019) 1–9.
[45] M. Nguyen, D. Lallemant, Order matters: the benefits of ordinal fragility curves for damage and loss estimation, Risk Anal. 42 (2022) 1136–1148.
[46] J.G. Rots, P.A. Korswagen, M. Longo, Computational Modelling Checks of Masonry Building Damage due to Deep Subsidence, Delft University of Technology, 2021.
[47] P.A. Korswagen, M. Longo, E. Meulman, C. van Hoogdalem, Damage Sensitivity of Groningen Masonry structures–experimental and Computational Studies: Stream 1, 2017.
[48] P. Van Staalduinen, J. Rots, K. Terwel, Onderzoek Naar De Oorzaken Van Bouwkundige Schade in Groningen: Methodologie En Case Studies Ter Duiding Vande Oorzaken, 2019.
[49] A. Prosperi, Modelling of Subsidence Induced Damage to Masonry Buildings: Influence of Soil Heterogeneity on Settlement and Development of Fragility Curves, Delft University of Technology, 2025.
[50] NPR 9096-1-1:2012 nl, Steenconstructies - Eenvoudige Ontwerpregels, Gebaseerd Op NEN-EN 1996-1-1+C1 (*Masonry Structures - Simple Design Rules, based on NEN-EN 1996-1-1+C1*), 2012.
[51] B. Standard, Eurocode 6—Design of Masonry structures—, British Standard Institution, London, 2005.
[52] G. Schreppers, A. Garofano, F. Messali, J. Rots, DIANA validation report for masonry modelling, DIANA FEA report (2016).
[53] J. Rots, F. Messali, R. Esposito, S. Jafari, V. Mariani, Thematic keynote computational modelling of masonry with a view to Groningen induced seismicity. Structural Analysis of Historical Constructions: Anamnesis, Diagnosis, Therapy, Controls: Proceedings of the 10th International Conference on Structural Analysis of Historical Constructions (SAHC, Leuven, Belgium, 13-15 September 2016), CRC Press, 2016, pp. 227–238.
[54] NPR9998:2020en, Assessment of Structural Safety of Buildings in Case of Erection, Reconstruction and Disapproval - Induced Earthquakes - Basis of Design, Actions and Resistances, 2021.
[55] S. Jafari, J.G. Rots, R. Esposito, F. Messali, Characterizing the material properties of dutch unreinforced masonry, International Conference on Analytical Models and New Concepts in Concrete and Masonry Structures 193 (2017) 250–257.
[56] NEHRP, NIST GCR 12-917-21 soil–structure Interaction for Building Structures, National Institute of Standards and Technology, US Department of Commerce, Gaithersburg, 2012.
[57] G. Gazetas, Foundation Vibrations. Foundation Engineering Handbook, Springer, 1991, pp. 553–593.
[58] J. Rots, Structural Masonry: an experimental/numerical Basis for Practical Design Rules, 1994.
[59] P.J.B.B. Lourenço, Computational Strategies for Masonry Structures, 1997.
[60] M. Longo, M. Sousamli, P.A. Korswagen, P. van Staalduinen, J.G. Rots, Sub-structure-based 'three-tiered' finite element approach to soil-masonry-wall interaction for light seismic motion, Eng. Struct. 245 (2021) 112847.
[61] M.D. Boscardin, E.J. Cording, Building response to excavation-induced settlement, J Geotech Eng-Asce. 115 (1989) 1–21.
[62] R.B. Peck, Deep excavations and tunneling in soft ground, Proc 7th ICSMFE 1969 (1969) 225–290.
[63] J. Fuertes, Calibrated Numerical Models for Masonry Buildings Subjected to subsidence-related Ground Settlements, Delft University of Technology, 2024.
[64] J.A. Charles, H.D. Skinner, Settlement and tilt of low-rise buildings, P I Civil Eng-Geotec 157 (2004) 65–75.
[65] G. Grünthal, European macroseismic scale 1998. European Seismological Commission (ESC), 1998.
[66] M. Sousamli, Orthotropic Cyclic Continuum Constitutive Model for Masonry Structures and Comparative Studies, 2024.
[67] CEN, Eurocode 7 Geotechnical Design - Part 1: General Rules. Final Draft, EN 1997-1:2004 (E), (F) and (G), European Committee for Standardization, 2004, p. 168. Brussels.
[68] M. Korff, Deformations and damage to buildings adjacent to deep excavations in soft soils, Delft Cluster (2009).
[69] J.N. Franzius, Behaviour of Buildings due to Tunnel Induced Subsidence, Imperial College London (University of London), 2004.
[70] D.M. Potts, T.I. Addenbrooke, A Structure's Influence on tunnelling-induced Ground Movements, vol 125, P I Civil Eng-Geotec, 1997, pp. 109–125.
[71] K.H. Goh, R.J. Mair, Building damage assessment for deep excavations in Singapore and the influence of building stiffness, Geotech. Eng. 42 (2011) 1–12.
[72] P.A. Korswagen, M. Longo, J.G. Rots, Research into the Combined Effects of Soil Strains, Soil Curvatures and Earthquake Vibrations from Multiple Mining Activities on Damage in Masonry, 2024.
[73] L.M. Zhang, A.M.Y. Ng, Probabilistic limiting tolerable displacements for serviceability limit state design of foundations, Geotechnique 55 (2005) 151–161.
[74] O. Mavrouli, S. Fotopoulou, K. Pitilakis, G. Zuccaro, J. Corominas, A. Santo, et al., Vulnerability assessment for reinforced concrete buildings exposed to landslides, Bull. Eng. Geol. Environ. 73 (2014) 265–289.
[75] C. Negulescu, E. Foerster, Parametric studies and quantitative assessment of the vulnerability of a RC frame building exposed to differential settlements, Nat Hazard Earth Sys 10 (2010) 1781–1792.